Serveur Académique Lausannois SERVAL serval.unil.ch

Author Manuscript
Faculty of Biology and Medicine Publication

This paper has been peer-reviewed but dos not include the final publisher proof-corrections or journal pagination.

Published in final edited form as:

Title: Pharmacological eEF2K activation promotes cell death and inhibits cancer progression.
Authors: De Gassart A, Demaria O, Panes R, Zaffalon L, Ryazanov AG, Gilliet M, Martinon F
Journal: EMBO reports
Year: 2016 Oct
Volume: 17
Issue: 10
Pages: 1471-1484
DOI: 10.15252/embr.201642194

In the absence of a copyright statement, users should assume that standard copyright protection applies, unless the article contains an explicit statement to the contrary. In case of doubt, contact the journal publisher to verify the copyright status of an article.

serval
serveur académique lausannois

UNIL | Université de Lausanne
Faculté de biologie et de médecine

Pharmacological eEF2K activation promotes cell death and inhibits cancer progression.

Authors: Aude De Gassart[1], Olivier Demaria[2], Rébecca Panes[1], Léa Zaffalon[1], Alexey G. Ryazanov[3], Michel Gilliet[2] and Fabio Martinon[1]*

Affiliations:

[1] Departement of Biochemistry, University of Lausanne, Epalinges 1066, Switzerland.

[2] Department of Dermatology, CHUV, Lausanne 1011, Switzerland.

[3] Department of Pharmacology, Rutgers The State University of New Jersey, Robert Wood Johnson Medical School, Piscataway, New Jersey 08854, USA.

*Correspondence to:

Fabio Martinon,
Departement of Biochemistry
University of Lausanne,
Ch. Des Boveresses 155
Epalinges 1066, Switzerland
Phone: +41-21-692.5695
Email: Fabio.Martinon@unil.ch

Conflicts of interest statement: The authors disclose no conflicts of interest.

Running title: Anti-tumoral properties of eEF2K over-activation

Keywords: Cancer, eEF2K, mRNA translation, cell death, HIV-protease inhibitors

Number of Figures: 6 (plus 5 EV Figures, 5 Appendix supplementary Figures and 1 EV Dataset)

Short Two sentence summary:

EEF2K is part of an adaptation pathway that help cells cope with lack of nutrients by regulating translation rates. Pharmacological over-activation of the eEF2K pathway with the anti-viral drug Nelfinavir rewires this survival stress-adaptation program into a response that is detrimental for tumor growth.

Bullet Points:

- The anti-viral and anti-tumoral molecule Nelfinavir is a potent eEF2K activator
- EEF2K activation contributes to NFR-mediated cell death
- EEF2K deficiency impairs Nelfinavir mediated antitumoral activity

Abstract:

Activation of the elongation factor 2 kinase (eEF2K) leads to the phosphorylation and inhibition of the elongation factor eEF2, reducing mRNA translation rates. Emerging evidence indicates that regulation of factors involve in protein synthesis may be critical for controlling diverse biological processes including cancer progression. Here we show that the inhibitors of the HIV aspartyl protease (HIV-PIs), Nelfinavir in particular, trigger a robust activation of eEF2K leading to the phosphorylation of eEF2. Beyond its anti-viral effects, Nelfinavir has antitumoral activity and promotes cell death. We found that Nelfinavir-resistant cells specifically evade eEF2 inhibition. Decreased cell viability induced by Nelfinavir was impaired in cells lacking eEF2K. Moreover, Nelfinavir mediated anti-tumoral activity *in vivo* was severely compromised in eEF2K-deficient engrafted tumors. Our findings imply that exacerbated activation of eEF2K is detrimental for tumor survival and describe a mechanism behind the anti-tumoral properties of the HIV-PIs.

Introduction:

Drug repositioning is emerging as a successful strategy that accounts for a significant share of newly US Food and Drug Administration (FDA)-approved drugs in recent years [1] [2]. The study of unanticipated drugs effects in patients can uncover new pathways and mechanisms of biological interest that can contribute to the development of new therapeutics. Early studies in HIV patients treated with the HIV aspartyl protease inhibitors (HIV-PIs) have suggested interesting off-target actions of these molecules in cancer [3-5]. The HIV-PIs target the viral protease and are widely used to treat HIV. In 1997 Nelfinavir (NFR) became one of the first HIV-PI to be approved by the FDA for HIV treatment. In addition to its anti-retroviral effects, this safe and orally available drug shows promising anti-tumoral activity in mice and humans [6-10]. Several phase I and phase II clinical trials are investigating the efficacy of NFR repositioning in cancer with encouraging initial results [11-15]. NFR has been shown to affect multiple pathways regulating cellular homeostasis including the proteasome, the kinase AKT and the Unfolded Protein Response (UPR) [16]. Recently we found that NFR is a robust inducer of the Integrated Stress Response (ISR), an adaptation response that promotes an ATF4-dependant transcriptional program [17]. While some of these pathways may contribute to its anti-tumoral activity, none has been demonstrated to be essential and the molecular basis of NFR mediated anti-tumoral effects remains unknown [16, 18, 19].

In this study we generated clonal populations of cells with increased resistance to NFR-mediated toxicity. These clones showed an unaltered activation of most NFR-mediated responses, including those related to the ISR. However, among possible stress and survival pathways, we observed the downregulation of the eukaryotic translation elongation factor 2 kinase (eEF2K), suggesting that it could be a major player driving Nelfinavir cytotoxic effects.

Activation of eEF2K is one of the pathways that participate to the restoration of cellular homeostasis upon conditions of nutrient or energy depletion by decreasing translation rates at the stage of elongation [20-23]. Indeed, the eEF2K activity inhibits the translation elongation factor eEF2, which mediates GTP-dependent translocation of the ribosome, thereby promoting peptide chain formation. In the tumoral context, increased activation of eEF2K downstream of mTORC1 inhibition by rapamycin, has been linked to APC-deficient adenoma growth arrest suggesting that enhancing eEF2K activity can be beneficial in patients with colorectal cancer [24].

Here, we report that the anti-cancer molecule NFR triggered a robust eEF2K-dependent eEF2 phosphorylation leading to decreased rates of translation elongation. We found that NFR-mediated eEF2K activation decreased cell proliferation and promoted cell-death. Consistent with these observations, we demonstrated in an *in vivo* model of engrafted tumors that NFR-mediated anti-tumoral activity is eEF2K dependent. Taken together these data indicate that the eEF2K pathway can be therapeutically manipulated to drive a response that is detrimental for tumor survival.

Results:

Nelfinavir resistance correlates with decreased eEF2K expression

Long-term treatment of immortalized cells with NFR is toxic and triggers cell death [10]. To get insight into the mechanisms involved, we treated HeLa cells with 10 μM of NFR and selected and characterized clones that survived and proliferated in presence of the drug (Fig 1A). NFR concentration can reach up to 17 μM in the plasma of treated patients [25, 26] and around 10 μM in liver tissues of mice that receive a dose of NFR reproducing the plasma concentration measured in patients [17]. Up to these concentrations of NFR we can observe a significant

increased viability in the resistant clones compared to the parental population (Fig 1B). We compared by RNA sequencing (RNA-seq), parental cells treated with NFR and four clones maintained in presence of the drug (Dataset EV1). We observed that many genes involved in ribonucleoprotein complex biogenesis and mRNA translation regulation were downregulated in the resistant clones compared to NFR treated parental cells. Among the translation-regulating pathways significantly down-regulated in the resistant clones we noticed the decrease of the *eukaryotic elongation factor 2 kinase* (*eEF2K*) mRNA. This finding was confirmed by real-time PCR (Fig 1C) and at the protein level by Western blot (Fig 1D). Then, we interrogated eEF2K expression in the clones following NFR withdraw. We found that in two out of three representative clones eEF2K downregulation was stable and maintained for more than three weeks in absence of NFR (Fig EV1). This indicated that decreased eEF2K expression was not a direct consequence of prolonged treatment with NFR, but could be the result of a selective advantage in a few cells that bypassed NFR-mediated cell death. This hypothesis implied that eEF2K could be engaged by NFR to decrease viability.

Nelfinavir triggers eEF2K to promote eEF2 phosphorylation

EEF2K controls the rate of translation elongation through the phosphorylation of the eukaryotic elongation factor 2 (eEF2) at threonine 56 (Thr^{56}). We therefore tested whether NFR can activate eEF2K by monitoring eEF2 phosphorylation. Short-term treatment with increasing concentrations of NFR triggered the phosphorylation of eEF2 in HeLa cells (Fig 2A). As expected, eEF2 phosphorylation was absent in eEF2K deficient mouse embryonic fibroblasts demonstrating that NFR engages eEF2K to regulate eEF2 (Fig 2B and Fig EV2A). EEF2K deficiency did not affect other pathways modulated by NFR [17], including the phosphorylation of the translation initiation factor eIF2α or the expression of ATF4 (Fig EV2A). Similarly

impairing eIF2α phosphorylation and therefore the Integrated Stress Response (ISR) did not affect NFR-mediated eEF2 regulation (Fig EV2B), suggesting that these two pathways are engaged independently one from the other. Then, we characterized these responses in the NFR resistant clones. NFR was withdrawn from the culture media for a few hours, and the NFR response was analyzed at 6 h of treatment. As expected, the clones showed a diminished expression of eEF2K protein that correlated with a reduced eEF2 phosphorylation in presence of low doses of NFR (Fig 2C and Fig EV3A). However, other pathways triggered by NFR such as the induction of ATF4 (Fig EV3B) were not affected in NFR resistant clones, which even expressed high level of NFR-response markers such as CHOP or DNAJB9 (Fig EV3C).

Investigation of a panel of HIV-PIs used in the clinic as well as hydroxy-t-butylamidenelfinavir (M8), the active NFR metabolite, showed that most HIV-PIs trigger eEF2 phosphorylation (Fig 2D). Yet, we consistently found that among the HIV-PIs, NFR is the most robust inducer of this pathway at relevant concentrations.

Nelfinavir does not inhibit the mTORC1 pathway to promote eEF2K activation

EEF2K activity is regulated by phosphorylation, which occurs at several sites downstream of specific signaling pathways. In particular, the mTORC1 downstream p70 S6 kinase negatively regulates eEFK by promoting its phosphorylation at inhibitory sites thereby allowing translation to proceed [20] and AMP-activated protein kinase (AMPK), a sensor of low energy status, has been shown to promote activator phosphorylation of eEF2K [27] (Fig 3A). Inhibition of mTORC1 with chemical inhibitors such as rapamycin or the starvation-induced activation of AMPK impairs eEF2K phosphorylation leading to its activation and inhibition of eEF2 [28, 29]. Because many phosphorylation sites have been shown to regulate eEF2K [30], we separated cell extracts on a phos-tag SDS-PAGE to get a comprehensive analysis of its

phosphorylation status. No significant changes on the eEF2K phosphorylation pattern were detected in presence of NFR while rapamycin or starvation considerably affected the overall eEF2K phosphorylation (Fig EV3D). In line with these observations, the dephosphorylation of the mTORC1 effectors S6 ribosomal protein or 4EBP1, a hallmark of mTORC1 inhibition and treatment with rapamycin, were only minimally affected in presence of NFR (Fig 3B, compare lanes 2-4 with 6-7). Importantly this effect was not observed in eEF2K deficient cells (Fig 3B**,** compare lane 2-4 with lanes 14-16), suggesting that NFR only slightly affects the mTORC1 pathway downstream of eEF2K activation. Independence from mTORC1 was also confirmed by the observation that rapamycin, that does not trigger a strong eEF2 phosphorylation *per se*, did not affect NFR-mediated eEF2 phosphorylation (Fig 3C**).** AMPK activation has been shown to trigger eEF2K activation both indirectly through mTORC1 inhibition and directly by phosphorylating eEF2K [27]. Indeed, the AMPK agonist AICAR is a potent inducer of eEF2K dependent eEF2 phosphorylation (Fig 2B and 3B). Interestingly we observed that concentrations above 20 μM of NFR triggered AMPK phosphorylation (Fig 3B, lane 3,4 and 15,16) suggesting that this pathway could be involved in mediating NFR responses. Yet, deletion of both AMPK isoforms α1 and α2 did not affect NFR-induced eEF2 phosphorylation whereas it impaired AICAR response (Fig 3D). AKT has been shown to be a target of NFR [10, 31, 32]; we therefore monitored AKT phosphorylation. Upon treatment with NFR we did not observe decreased basal AKT phosphorylation (Fig 3B). Moreover inhibition of AKT with the selective inhibitor MK-2206 did not affect NFR-mediated eEF2 phosphorylation (Fig EV3C). Similarly inhibition of AKT phosphorylation upon treatment with the Phosphoinositide 3-kinase (PI3K) inhibitors 3-Methyladenine (3MA) and Wortmanin did not affect NFR-induced eEF2 phosphorylation

(Appendix Fig S1). Altogether these data demonstrate that NFR signals eEF2K activation independently of the eEF2K activating pathways mTORC1 inhibition, AMPK or the ISR.

eEF2K activation contributes to decreased translation rates

To quantify the role of eEF2K in NFR-mediated translation inhibition, we measured global translation rates using ^{35}S-labelled methionine incorporation. We found that eEF2K deficiency partially rescued NFR mediated decreased translation rates without impacting on tunicamycin-mediated regulation of translation (Fig 4A, 4B). In these cells rapamycin triggered a relatively weak eEF2 phosphorylation (Fig 2B), thus, eEF2K did not significantly contribute to rapamycin-mediated translation decrease (Fig 4B). Similar to eEF2K deficiency, impairing eIF2α phosphorylation partially restored methionine incorporation, indicating that both pathways contribute to NFR-mediated reprograming of mRNA translation (Fig 4B). We also examined the role of eEF2K in NFR mediated mRNA translation control by measuring polysomal distribution. Treatment with NFR resulted in a decrease of mRNA associated to polysomes and an increase of free ribosomes, overall reflecting a decrease of protein synthesis, whereas eEF2K deficiency reversed this effect (Fig 4C). On the contrary, treatment with the ER-stress inducer tunicamycin, triggered a decrease of the polysomal fraction that was unaffected by eEF2K deficiency but was rescued in presence of the ISR inhibitor ISRIB or in cells unable to phosphorylate eIF2α (Fig EV4A , EV4B). Inhibiting the ISR did not significantly affect the NFR-mediated decrease in polysomes (Fig EV4A , EV4B). Interestingly while NFR clearly affected the polysomal profile in an eEF2K dependent manner, we did not observe the expected increase of the polysomal fraction that is predicted to accumulate upon elongation defects as observed in presence of cycloheximide, a molecule that exerts its effect by interfering with the translocation step in protein synthesis (Fig EV4C). Instead we observed a decreased polysomal fraction and increased

free ribosomes signal. This indicates that specific eEF2K activation and eEF2 phosphorylation may affect additional steps in the translation program beyond its function during elongation. Previous report have suggested that eEF2 could be involved in the splitting of the 80S ribosomes into subunits, a process required for the initiation steps of translation [33].

The observation that eEF2K deficiency restored the polysomal fraction clearly underlined the key role of this pathway in regulating translation by NFR. However this observation is in apparent contradiction with the fact that eEF2K only partially restored overall protein synthesis (Fig 4A, 4B). A similar observation was made upon treatment with rapamycin (Fig 4B, EV4C). It is therefore possible that concomitant regulation of both the initiation and elongation machineries may mask the contribution of each mechanism on the polysomal traces. We therefore tested eEF2K contribution to elongation by examining NFR regulation of the ribosome half-transit time [34]. This was performed by measuring the kinetics of radioactive amino acid incorporation into total protein in post-mitochondrial supernatant (PMS) and into completed polypeptides released from the ribosome in post-ribosomal supernatant (PRS). The average half-transit time was determined from the displacement in time between the two lines corresponding to the PMS and PRS data plotted as a function of time (Fig. 4D). We measured that NFR significantly increased the ribosome half-transit time. This effect on elongation was not observed in eEF2K deficient cells indicating that eEF2K negatively regulate polypeptide elongation rates in presence of NFR.

Overall these experiments define eEF2K activation as a key pathway of NFR-mediated protein synthesis regulation and indicate that eEF2K beyond it function as a regulator of elongation, can affect polysomes by a mechanism that is yet to be identified.

eEF2K activation decreases proliferation and promotes cell death

The observation that loss of eEF2K may confer a fitness advantage to the cells in presence of NFR (Fig 1B) prompted us to interrogate whether sustained eEF2K activation could affects cell growth and contribute to NFR-mediated cell death. To test this hypothesis we measured cell viability and proliferation in NFR treated eEF2K deficient MEFs and control cells. Consistently we found that NFR-mediated decreased proliferation was affected by eEF2K deficiency in presence of 10 μM NFR (Fig 5A). We performed genome editing by means of CRISPR/Cas9 to inactivate the *eEF2K* gene in additional cell lines (Appendix Fig S2A-C**)**. Loss of eEF2K affected NFR-mediated growth inhibition in all populations tested including those isolated from HeLa (Appendix Fig S2D), A549 (Appendix Fig S2E) and MCF7 cells (Fig Appendix Fig S2F). Moreover reconstitution of eEF2K -/- MEFs with a construct expressing the kinase (Appendix Fig S2G), restored NFR responses to the levels observed in wild-type cells (Fig 5A). We also monitored eEF2K role in mediating NFR toxicity by analyzing cell viability by MTS assay upon increasing doses of NFR. We found that eEF2K deficiency decreased sensitivity to NFR (Fig 5B). This was mostly striking at physiological concentrations below 20 μM. As reported for the growth defect, reconstitution with eEF2K restored full NFR toxicity (Fig 5C). Similar findings were found in the eEF2K-deficient cell lines tested (Fig 5D, E, and F). Next we interrogated NFR-mediated cell death by quantifying dying cells using annexin V and propidium iodide (PI) staining after 24h of treatment. In line with the results obtained by monitoring NFR sensitivity, we found that eEF2K deficiency decreased NFR-mediated cell death and that reconstitution of eEF2K deficient cells with eEF2K restored the response to NFR (Fig 5G and Appendix Fig S3)

EEF2K deficiency did not confer a promiscuous resistance to cell death as demonstrated by unaltered loss of viability in presence of other compounds such as tunicamycin (TM) or the

apoptosis-inducing drug staurosporine (Appendix Fig S4). Other pathways including those related to the ISR are activated by NFR and could affect cell viability [7, 10, 17, 35]. Cells deficient in key signaling components of the UPR pathway including PERK, ATF4, IRE1, XBP1 and cells unable to phosphorylate eIF2α were tested for NFR-sensitivity. Compared to control cells, no alteration in cell death was observed in these deficiencies (Fig EV5). All together these observations demonstrate that sustained activation of eEF2K affects cell viability and contributes to cell death and growth inhibition in presence of NFR, in particular at physiologically relevant concentrations of the drug; below 20 μM.

Pharmacological over-activation of eEF2K reduces tumor growth

To determine the relevance of eEF2K in mediating NFR therapeutic effects *in vivo*, RasV12-transformed proficient or eEF2K deficient MEFs were generated to transplant tumors into AGR129 (IFN-α/β, IFN-γ receptor and RAG-2 deficient) mice [36]. Transformation did not significantly affect eEF2K activation (Appendix Fig S5A) or its role in mediating NFR susceptibility (Appendix Fig S5B). Mice were injected subcutaneously with eEF2K deficient cells on one flank and eEF2K proficient cells on the other flank. As reported previously in *nu/nu* immunocompromised mice [37], eEF2K deficiency did not affect overall tumor formation and growth in feed animals (Fig 6A). At day 6 post-implantation, a daily treatment with NFR was started. This resulted in growth inhibition of WT tumor, but strikingly did not affect the growth of eEF2K deficient tumors (Fig 6A). As expected, NFR treatment increased eEF2 phosphorylation in post-mortem tumor biopsies (Fig 6B and C), indicating that sustained eEF2K mediated eEF2 inhibition is a key factor contributing to the anti cancer properties of NFR *in vivo*.

Discussion:

We have previously shown that NFR triggers a transcriptional program that mostly rely on the ISR [17]; however here we found that this pathway is not a main player driving NFR-mediated toxicity. Indeed, we showed that NFR-resistant clones could survive and proliferate for weeks in presence of the drug despite robust and sustained ISR activation. In addition, transgenic cells unable to activate ISR are not protected against NFR toxicity. In contrast, we found that NFR-mediated toxicity relies on translation reprograming rather than transcriptional responses. Mechanistically, this was mediated at least in part by activation of eEF2K, a stress response kinase that regulates translation programs. This pathway was downregulated in NFR-resistant clones. Moreover, a decreased sensitivity to NFR and an impaired growth inhibition was observed in cells with eEF2K deficiency. In mice, we found that the anti-tumoral effects of NFR are eEF2K-dependent, demonstrating that overactivation of this pathway within cancer cells can affect tumor growth. NFR ability to trigger eEF2K signaling was comparable in all human and mouse cell types tested indicating that this pathway is a conserved hallmark of NFR-mediated stress response. It is therefore reasonable to predict that this response could be part of the NFR anti-tumoral effects observed in cancer patients [10-12].

The activation of eEF2K is part of an adaptation program that may help stressed cells, such as cancer cells, to cope with conditions of low nutriment and energy [38]. This was shown for example in eEF2K deficient tumors that were found to be more sensitive to caloric restriction [37]. Moreover inhibition of eEF2K suppresses growth of Pten/p53-deficient Triple-negative breast cancer (TNBC) with elevated Akt signaling xenografts *in vivo* [39]. Down-modulation of eEF2K in breast cancer cell lines has also been reported to decrease the expression of oncogenes such as c-Myc, thereby impacting on survival and growth [23]. These findings clearly indicate

that eEF2K activation is a hallmark of stressed cells within tumors. Accordingly, it was proposed that an AMPK-eEF2K-dependent reduction of global translation could contribute to preserving energy and conferring tolerance to stress in cancer cells [38, 40]. Our observations that increased activation of eEF2K may signal cell death and decreased growth could be in apparent contradiction with its role as part of an adaptation program. However, deregulated or prolonged stress signals can also turn adaptation programs into programed cell death aimed at eliminating irremediably damaged cells. This scenario was demonstrated in the context of several stress pathways including during ER-stress [41]. It is therefore possible that eEF2K integrates signals that promote survival or death depending on the level or duration of its activation status. By increasing eEF2K activity, NFR may redirect the eEF2K program toward death. EEF2K activation observed in stressed tissues as part of the adaptation program may increase their sensitivity to the drug compared to healthy tissues. The status of eEF2K activation within the tumor may therefore influence NFR responsiveness and should be considered as a potential biomarker that could indicate NFR as a therapeutic choice.

The finding that pharmacological eEF2K activation could be detrimental for optimal tumor growth is also supported by a study investigating rapamycin effects in a mouse model of colon cancer that reported that rapamycin-mediated APC-deficient adenoma growth arrest required eEF2K [24]. Rapamycin inhibits the mTORC1 complex, a master regulator that integrates the signals from nutrient and energy sensors with cell growth. Expression of many mRNA encoding oncogenes or growth promoting factors has been show to be translationally regulated downstream of mTOR activity [42]. Interestingly, mTOR can modulate both initiation and elongation phase (respectively through 4EBP-1-eIF4E and p70 S6K-eEF2K-eEF2 downstream effectors) of mRNA translation to facilitate cell proliferation. The discovery that

mTOR inhibition is detrimental for tumor development in an eEF2K dependent manner raises the possibility that modifying the translational landscape by targeting elongation factors could be a promising strategy to decrease tumor growth. Nevertheless, therapeutic approaches aimed at targeting mTORC1 relies on a complex network of regulatory loops that affects its function impacting on cancer progression but also leading to increase numbers of potential side effects [43]. In contrast, NFR does not significantly affect the mTORC1 signaling pathway and therefore represents a new valuable tool to study and specifically promote eEF2K activation *in vitro*, in mice as well as in patients. In this study we show that eEF2K activating pathways such as mTORC1 inhibition, AMPK or the ISR were not involved in NFR-mediated eFF2K activation. Possible alternative pathway that could contribute to NFR-mediated effects include calcium ion influx, hypoxia or ERK signaling that have been proposed to regulate eEF2K [44]. It is likely that the identification of NFR cellular targets and mechanism of action will shed new light on novel pathways that can drive eEF2K activation. These mechanisms are predicted to be complex, and may involve NFR binding to multiple targets [19]. Moreover, despite the fact that we do not observe eEF2K activation with the HIV-PIs Amprenavir, we cannot exclude that some aspects of the HIV-PIs response could be related to the peptidometic nature of these molecules [45].

How increased eEF2K activation may affect proliferation and promote death is an important question that remains to be solved. It is possible that eEF2K activation may lead to exceed the acceptable threshold of overall translation inhibition or may specifically alter the repertoire of translated genes by preferentially affecting survival and proliferation factors. Malignant cells exhibit altered translational programming that is characterized by augmented activity of many components of the translation machinery, leading to increased overall protein

synthesis and modulation of specific oncogenic networks [46]. This was shown for example in mice engineered to carry only a single copy of the translation initiation factor *eIF4E* gene [47]. These mice develop normally and show a functional translation machinery at basal. However, oncogenic transformation and tumorigenesis was affected by decreased eIF4E levels indicating that tumors rely on maximal translation capacity [47]. Therefore, therapeutic agents that target components of the translation machinery to decrease translation rates hold promise as broad activity anticancer drugs that could overcome intra-tumor heterogeneity [48]. NFR, by inhibiting eEF2, can decrease global rates of protein synthesis and possibly affect the translation of specific mRNAs that could promote tumor cell survival and proliferation. This activity likely contributes to the antitumoral effects and decreased cell growth observed upon eEF2K activation.

In conclusion, the data presented in this study highlight the importance of eEF2K as a therapeutic target in cancer and identify NFR, a well-known drug with a relatively safe profile and oral bioavailability, as an anti-cancer treatment that over-activates eEF2K to limit tumor viability. These data further suggest that in addition of being interesting targets for inhibition, stress responses and adaptation programs can be manipulated to provide increased signal that can lead to cell death and the elimination of stressed cancer tissues.

Materials and Methods

Cell culture and Drug Treatment.

Each knockout or transgenic Mouse Embryonic Fibroblast (MEF) cell line was compared to littermate control. EEF2K WT and KO MEF were provided by A.G. Ryazanov. EIF2αWT and eIF2αS51A MEF were from RJ. Kaufman (Sanford Burnham Medical Research Institute, La Jolla, CA, USA). MEF IRE1-/-, XBP1-/-, PERK-/- and they respective WT controls were from

L. Glimcher (Weill Cornell Medical College, New York, USA). MEF ATF4-/- and ATF4+/+ were provided by A. Bruhat (INRA, Saint-Genes-Champanelle, France). AMPKα1α2 WT and double KO MEF were from B. Viollet (Institut Cochin, Université Paris Descartes, France). Cell lines have not been authenticated and are tested for mycoplasma once per year in the laboratory. Nelfinavir Mesylate (CAS 159989-65-8) was from Axon Medchem, LGM pharma; Ritonavir, Atazanavir, Lopinavir and Saquinavir were obtained from The NIH AIDS Reagent Program; Nelfinavir hydroxy-tert-butylamide (M8) was from Santa-Cruz (sc-208088). Tunicamycin (TM), Cycloheximide (CHX), AICAR (5-amino-1-β-D-ribofuranosyl-imidazole-4-carboxamide), MK-2206 and Rapamycin were from Enzo-Life Sciences. Doxycycline, Staurosporine, Wortmanin and 3-MA were from Sigma-Aldrich. For starvation condition cells were maintained for 1h in PBS.

Immunoblot analysis.

Every WB shown in the study is representative of at least three independent experiments performed in same conditions. Cells and tumor protein extracts were prepared with RIPA buffer (50 mM NaCl, 50 mM TRIS pH-7,4, 1 mM EDTA, 0.1% SDS, 1% NP40, 1% Sodium Deoxycholate) supplemented with Proteases inhibitors cocktail (Roche), 10 mM Na3VO4, 50mM NaF, 10mM Na4P2O7 and 5 μM MG132 (Sigma-Aldrich). The following antibodies were used for immunoblot analysis: anti-EEF2K (Cell Signaling; #3692); anti-phospho-EEF2^{T56} (Cell Signaling; #2331); anti-total-EEF2 (Cell Signaling; #2332); anti-phospho-S6 Ribosomal protein$^{S240/244}$ (Cell Signaling; #2215); anti-total-S6 Ribosomal protein (Cell Signaling; #2317); anti-phospho-Akt^{T308} (Cell Signaling; #9275), anti-total-Akt (Cell Signaling; #9272), anti-phospho-AMPKα^{T172} (Cell Signaling; #2535), anti-total-AMPKα (Cell Signaling; #2793S), anti-4EBP1 (Cell Signaling; #9644); anti-ATF4 (Santa Cruz; sc-200), anti-phospho-eIF2α (Cell

Signaling; #3597S), anti-total-eIF2α (Cell Signaling; #9722S); anti-Tubulin (Adipogen; F2C). WB quantifications were performed using ImageJ software.

***Polysomal profiling*.**

Cells were treated with 20 μM NFR, 10 μg/ml Tunicamycin or DMSO for 6h. Culture medium was removed and cells were harvested using cold PBS supplemented with 5 mM EDTA and 100 μg/ml Cycloheximide (CHX). After two washes in cold PBS containing 100 μg/ml CHX, pellets were resuspended with hypotonic buffer (1.5 mM KCl, 2.5 mM MgCl2, 5 mM Tris pH7.4) supplemented with 0.1 μg/ml Heparin, 100 μg/ml CHX, 20 U/ml RNAsin, and proteases inhibitors. Equal amount of lysis buffer (Hypotonic buffer 2% DOC, 2% TritonX100, 2.5 mM DTT) was added and subsequent cell lysates were vigorously vortexed, incubated 20 minutes on ice and centrifuged at 13000 r.p.m. for 10 minutes at 4°C. Post-nuclear lysates were layered on 10 ml 10–50% (w/v) sucrose gradients (50, 40, 30, 20, 10% sucrose in 80 mM NaCl, 5 mM MgCl2, 20 mM Tris pH7.4, 1 mM DTT and 100 μg/ml CHX in DEPC H2O). Gradients were centrifuged at 30,000 r.p.m. for 4h at 4 °C and separated through a live OD254 nm ultraviolet spectrometer. Comparison of polysomal (P) and subpolysomal (S) abundance was based on the measurement of area under the curve. All experiments were repeated at least two times in same conditions. P/S ratio were calculated for each condition and normalized to DMSO treated cells.

Metabolic labeling.

Cells were treated for indicated times with NFR, 200nM Rapamicin, 1μg/ml Cycloheximide or 10 μg/ml TM and incubated for the last 15 minutes with a mixture of L-(35)S-Methionine/Cysteine (5 μCi/ml). Cells were washed with PBS and lysed with RIPA buffer. Samples were analyzed by autoradiography after SDS/PAGE separation or collected on a glass fiber filter (GF/C, Whatman). Filters were washed twice with ice-cold 10% TCA, once with 5%

TCA, rinsed twice with ethanol, and air-dried before being subjected to liquid scintillation counting. Values were normalized as percentage of Mock treated cells.

Ribosome Half-Transit Time Measurement.

Ribosome half-transit time measurements were assessed as in [37, 39] with the following modifications. 200 000 cells seeded for 24 hrs in 6 well plates were treated for 6 hrs with 20μM NFR; after 5.5 hrs treatment medium was replaced with labeling medium (DMEM. With 4500 mg/L glucose and sodium bicarbonate, without L-methionine, L-cystine and L-glutamine. [Sigma-Aldrich] supplemented with 10% FCS, 1% Non Essential Amino Acids (Gibco-Life Technologies™) and 2mM L-Glutamine (AMIMED, Bioconcept)) for 30 minutes before addition of 1μCi/well/ml of L-(35)S-Methionine/Cysteine. For Cycloheximide treatment, CHX was added at 1μg/ml to the labeling medium for 30 min. For starvation condition, cells were kept in PBS for 30 minutes before labeling. At indicated times (5, 7.5, 10, 12.5 and 15 minutes) after labeling, cells were washed twice in ice-cold PBS containing 100 μg/ml cycloheximide, and lysed by adding 250μl of RSB lysis buffer (10 mM NaCl; 10 mM Tris-HCl, pH 7.4; 15 mM MgCl2; 1% Triton X-100 and 100 μg/ml heparin) containing protease inhibitors directly into the well. Cell lysate were harvested, vortexed, and incubated on ice for 20 min. Nuclei and mitochondria were cleared by centrifugation at 13 000rpm for 10 min at 4°C. 250 μl post-mitochondrial supernatant (PMS) was mixed with an equal volume of polysomal buffer (25 mM Tris-HCl, pH 7.4; 10 mM MgCl2; 25 mM NaCl; 0.05% Triton X-100; 0.14 M sucrose; 500 μg/ml heparin) and 250 μl was removed to measure incorporation of [35S]-methionine and cysteine into total protein (nascent and completed). Polysomes were pelleted by centrifugation of the remaining supernatant at 55,000 g for 1 h at 4°C in a Beckman TLA120 rotor. 200 μl post-

ribosomal supernatant (PRS) was removed to measure the incorporation of [35S]-methionine and cysteine into completed proteins. 100 µl of PMS and PRS samples were collected on a glass fiber filter (GF/C, Whatman). Filters were washed twice with ice-cold 10% TCA, once with 5% TCA, rinsed twice with ethanol, and air-dried before being subjected to liquid scintillation counting. Incorporation of [35S]-methionine and cysteine into total protein within the PMS and PRS was obtained by linear regression analysis. Ribosome half transit time was calculated using the difference of x abscise values chosen for time of 300 sec.

Cytotoxic assay.

Cell viability was evaluated by using a 3-(4,5-dimethylthiazol-2-yl)-5-(3-carboxymethoxyphenyl)-2-(4-sulfonphenyl)-2H-tetrazolium (MTS) assay (Promega, Madison, WI). All experiments were done in triplicate and were repeated at least 3 times. The inhibition of cell proliferation was expressed as the percentage of vehicle control treated cells. Dose-inhibition rate curves were plotted using a five-parameter logistic equation. For all experiments EC50 value (the 50% maximal inhibitory concentration) was calculated and mean +/- s.e.m. of at least 3 independent experiments is shown.

Cell proliferation measurement.

1,000 cells were seeded in 96 well plates and let adhere for 24h. Just before drug addition, cells were counted on a define area of each well using a Spectramax imager technology in order to determine the number of cell at time 0. Cells were treated with vehicle or with 10 µM NFR and each well was imaged again at indicated times. The fold change of cell number compare to time 0 was calculated for each individual well at indicated time. Curves represented

the mean +/- s.e.m. of three different wells treated or not with 10 μM NFR. The percentage of growth inhibition, was determined using the ratio between growth of treated and untreated cells at 72h of NFR treatment. For every cell line, curves showed one representative of 3 experiments performed in triplicate in the same conditions and histograms are mean +/- s.e.m. of 3 independent experiments.

AnnexinV/PI staining and FACS analysis.

Annexin V/propidium iodide (PI) staining was performed using eBioscience Kit (BMS500FI) according to the manufacturer's guidelines. Briefly, $2x10^5$ cells plated in 12 well plates were treated for 24h with 0, 20 or 40 μM NFR. Cells and supernatant were harvested and centrifuged 5 minutes at 1200 r.p.m. Cells were washed in ice-cold PBS and resuspended in 50 μl of binding buffer containing 2.5 μl of AnnexinV-FITC and incubated for 30 minutes on ice. Cells were washed once and resupended in 100 μl of binding buffer containing 10 μl of PI (20μg/ml). Flow cytometric analysis was immediately performed using an Accuri flow cytometer Instrument (BD Bioscience).

Mice.

Animal experiments were approved by the Veterinary Office of the Canton de Vaud and the Animal Ethics Committee (authorization 2883). Immuno-compromised AGR 129 (IFN-α/β, IFN-γ receptor and RAG-2 deficient) mice were provided by M. Gilliet (Department of dermatology, CHUV, Lausanne) and housed at the University of Lausanne in accordance to local and national guidelines. $1x10^6$ MEF eEF2K WT-HRasV12 and eEF2K-/- HRasV12 were respectively injected subcutaneously into the right and left flank of six to eight-week-old female. Tumor growth was followed by measuring size of the tumor with a caliper. Tumor volume was

calculated using the formula $V=(Lxl^2)/2$. When tumors reach 200 mm3 mice were randomly distributed into two homogenous groups and injected intraperitoneally daily either with vehicle (4% DMSO, 5% PEG, 5% Tween 80 in saline) or with 100 mg/kg NFR. Experiments were repeated 2 times with 6 to 8 mice per group.

High-throughput sequencing.

For RNA sequencing, RNA was extracted using RNeasy mini Kit (QIAGEN) from 3 independent plates of HeLa cells treated or not with 20 μM NFR and from 4 independent 10 μM NFR resistant HeLa cells clones. High-throughput sequencing was performed at the Lausanne Genomics Technologies Facility (University of Lausanne) on the Illumina HiSeq 2500 using TruSeq SBS Kit v3 reagents. For the RNA-seq analysis, we used a moderated t-test from the R bioconductor package "limma" (R version 3.1.1, limma version 3.20.8). The "adjusted p-value", correspond to the p-values corrected for multiple testing using the Benjamini-Hochberg method.

RT-PCR.

SYBR Green fluorescent reagent and LightCycler480 Real time PCR System (Roche) were used for quantitative RT-PCR. Primer sequences used: EEF2K F,5'-CACCTGGAAGATATTGCCACC-3'; R,5'-GCTTCGCCACGTAGTTGGA-3'; EEF2 F,5'-AACTTCACGGTAGACCAGATCC-3'; R,5'-TCGTCCTTCCGGGTATCAGTG-3; DNAjB9 F,5'-TCTTAGGTGTGCCAAAATCGG-3' ; R,5'-TGTCAGGGTGGTACTTCATGG-3'; CHOP F,5'-GGAAACACAGTGGTCATTCCC-3'; F,5'-CTGCTTGAGCCGTTCATTCTC-3'. All RT-PCR were performed in experimental triplicate and repeated at least 3 times on independent samples.

Plasmid construction

LentiCRISPR-v2 for EEF2K targeting: Optimized CRISPR target sequences were cloned into the LentiCRISPR-v2 vector (Adgene #52961). The seed sequence was designed in the kinase domain of eEF2K as follows: CACCTGGAGCACTACATCGA. A sequence targeting luciferase was used as control sgRNA (CTTCGAAATGTCCGTTCGGT). p21-FlagEEF2K for EEF2K reconstitution: Human EEF2K was amplified by PCR from pDONR223-EEF2K (Addgene #23726) and, sub-cloned into Lentiviral pINDUCER21-plasmid (S. Elledge, Harvard Medical School).

Lentivirus production and cell line infection.

Lentiviruses were produced as previously described [17]. HeLa, A549 and MCF7 cells were infected with lentiCRISPR-v2 viruses targeting Luciferase or EEF2K. Positive populations were selected with 2 μg/ml puromycin. Clones were tested by WB for EEF2K protein level. MEF EEF2K-/- were infected with p21-FlagEEF2K viruses and GFP positive cells were FACS sorted 5 days after infection. Flag-EEF2K expression was induced using doxycycline (1 μg/ml for 24h). LZRS-H-rasV12 retroviruses used for MEF EEF2K WT and KO infections were provided by K. Lefort (GP Dotto laboratory, UNIL, Lausanne).

Statistical analysis.

Statistical significance was ascertained by performing appropriate tests described in figure legends. Significant differences were indicated by * ($p \leq 0.05$), ** ($p \leq 0.01$) or *** ($p \leq 0.001$). For the RNA-seq analysis, we used a moderated t-test from the R bioconductor package "limma".(R

version 3.1.1, limma version 3.20.8). The "adjusted p-value" reported in the Dataset S1, correspond to the p-values corrected for multiple testing using the Benjamini-Hochberg method, which controls for false discovery rate (FDR).

Acknowledgments: We thank L.H. Glimcher, A. Bruhat, R.J. Kaufman, B. Viollet, S. Elledge, C. Lefort, G.P. Dotto and the NIH AIDS Reagent Program for sharing key reagents. We thank Jérome Lugrin, Etienne Meylan, Owen Sansom and Margot Thome for critical reading of the manuscript. We thank Keith Harshman, Leonore Wigger and the staff of the Lausanne Genomics Technologies Facility for high-throughput sequencing. This project is supported by a grant from the European Research Council (ERC) starting grant (281996), a Human Frontier Science Program career development award (CDA00059/2011) and a grant from the Swiss National Science Foundation (31003A-130476).

Authors contribution: Conceptualization, F.M. and A.D.G.; Methodology, A.D.G., and F.M.; Investigation, A.D.G, O.D., R.P., B.A., and L.Z.; Writing – Original Draft, F.M. and A.D.G; Funding Acquisition, F.M.; Resources, A.G.R. and M.G.; Supervision, A.D.G., and F.M.

Conflicts of interest statement: The authors disclose no conflicts of interest.

References:

1. Ashburn TT, Thor KB (2004) Drug repositioning: identifying and developing new uses for existing drugs. *Nat Rev Drug Discov* **3**: 673-83
2. Jin G, Wong ST (2014) Toward better drug repositioning: prioritizing and integrating existing methods into efficient pipelines. *Drug Discov Today* **19**: 637-44
3. Lebbe C, Blum L, Pellet C, Blanchard G, Verola O, Morel P, Danne O, Calvo F (1998) Clinical and biological impact of antiretroviral therapy with protease inhibitors on HIV-related Kaposi's sarcoma. *AIDS* **12**: F45-9
4. Krischer J, Rutschmann O, Hirschel B, Vollenweider-Roten S, Saurat JH, Pechere M (1998) Regression of Kaposi's sarcoma during therapy with HIV-1 protease inhibitors: a prospective pilot study. *J Am Acad Dermatol* **38**: 594-8
5. Niehues T, Horneff G, Megahed M, Schroten H, Wahn V (1999) Complete regression of AIDS-related Kaposi's sarcoma in a child treated with highly active antiretroviral therapy. *AIDS* **13**: 1148-9
6. Cuneo KC, Tu T, Geng L, Fu A, Hallahan DE, Willey CD (2007) HIV protease inhibitors enhance the efficacy of irradiation. *Cancer research* **67**: 4886-93
7. Pyrko P, Kardosh A, Wang W, Xiong W, Schonthal AH, Chen TC (2007) HIV-1 protease inhibitors nelfinavir and atazanavir induce malignant glioma death by triggering endoplasmic reticulum stress. *Cancer research* **67**: 10920-8
8. Bernstein WB, Dennis PA (2008) Repositioning HIV protease inhibitors as cancer therapeutics. *Curr Opin HIV AIDS* **3**: 666-75
9. Bruning A, Burger P, Vogel M, Rahmeh M, Gingelmaiers A, Friese K, Lenhard M, Burges A (2009) Nelfinavir induces the unfolded protein response in ovarian cancer cells, resulting in ER vacuolization, cell cycle retardation and apoptosis. *Cancer Biol Ther* **8**: 226-32

10. Gills JJ, Lopiccolo J, Tsurutani J, Shoemaker RH, Best CJ, Abu-Asab MS, Borojerdi J, Warfel NA, Gardner ER, Danish M*, et al.* (2007) Nelfinavir, A lead HIV protease inhibitor, is a broad-spectrum, anticancer agent that induces endoplasmic reticulum stress, autophagy, and apoptosis in vitro and in vivo. *Clin Cancer Res* **13**: 5183-94
11. Chow WA, Jiang C, Guan M (2009) Anti-HIV drugs for cancer therapeutics: back to the future? *Lancet Oncol* **10**: 61-71
12. Blumenthal GM, Gills JJ, Ballas MS, Bernstein WB, Komiya T, Dechowdhury R, Morrow B, Root H, Chun G, Helsabeck C*, et al.* (2014) A phase I trial of the HIV protease inhibitor nelfinavir in adults with solid tumors. *Oncotarget* **5**: 8161-72
13. Rengan R, Mick R, Pryma D, Rosen MA, Lin LL, Maity AM, Evans TL, Stevenson JP, Langer CJ, Kucharczuk J*, et al.* (2012) A phase I trial of the HIV protease inhibitor nelfinavir with concurrent chemoradiotherapy for unresectable stage IIIA/IIIB non-small cell lung cancer: a report of toxicities and clinical response. *J Thorac Oncol* **7**: 709-15
14. Brunner TB, Geiger M, Grabenbauer GG, Lang-Welzenbach M, Mantoni TS, Cavallaro A, Sauer R, Hohenberger W, McKenna WG (2008) Phase I trial of the human immunodeficiency virus protease inhibitor nelfinavir and chemoradiation for locally advanced pancreatic cancer. *J Clin Oncol* **26**: 2699-706
15. Buijsen J, Lammering G, Jansen RL, Beets GL, Wals J, Sosef M, Den Boer MO, Leijtens J, Riedl RG, Theys J*, et al.* (2013) Phase I trial of the combination of the Akt inhibitor nelfinavir and chemoradiation for locally advanced rectal cancer. *Radiother Oncol* **107**: 184-8
16. Koltai T (2015) Nelfinavir and other protease inhibitors in cancer: mechanisms involved in anticancer activity. *F1000Res* **4**: 9
17. De Gassart A, Bujisic B, Zaffalon L, Decosterd LA, Di Micco A, Frera G, Tallant R, Martinon F (2015) An inhibitor of HIV-1 protease modulates constitutive eIF2alpha dephosphorylation to trigger a specific integrated stress response. *Proc Natl Acad Sci U S A*
18. Gantt S, Casper C, Ambinder RF (2013) Insights into the broad cellular effects of nelfinavir and the HIV protease inhibitors supporting their role in cancer treatment and prevention. *Curr Opin Oncol* **25**: 495-502
19. Xie L, Evangelidis T, Xie L, Bourne PE (2011) Drug discovery using chemical systems biology: weak inhibition of multiple kinases may contribute to the anti-cancer effect of nelfinavir. *PLoS Comput Biol* **7**: e1002037
20. Kenney JW, Moore CE, Wang X, Proud CG (2014) Eukaryotic elongation factor 2 kinase, an unusual enzyme with multiple roles. *Adv Biol Regul* **55**: 15-27
21. Ryazanov AG, Ward MD, Mendola CE, Pavur KS, Dorovkov MV, Wiedmann M, Erdjument-Bromage H, Tempst P, Parmer TG, Prostko CR*, et al.* (1997) Identification of a new class of protein kinases represented by eukaryotic elongation factor-2 kinase. *Proceedings of the National Academy of Sciences of the United States of America* **94**: 4884-9
22. Proud CG (2015) Regulation and roles of elongation factor 2 kinase. *Biochem Soc Trans* **43**: 328-32
23. Tekedereli I, Alpay SN, Tavares CD, Cobanoglu ZE, Kaoud TS, Sahin I, Sood AK, Lopez-Berestein G, Dalby KN, Ozpolat B (2012) Targeted silencing of elongation factor 2 kinase suppresses growth and sensitizes tumors to doxorubicin in an orthotopic model of breast cancer. *PLoS One* **7**: e41171
24. Faller WJ, Jackson TJ, Knight JR, Ridgway RA, Jamieson T, Karim SA, Jones C, Radulescu S, Huels DJ, Myant KB*, et al.* (2015) mTORC1-mediated translational elongation limits intestinal tumour initiation and growth. *Nature* **517**: 497-500
25. Hennessy M, Clarke S, Spiers JP, Kelleher D, Mulcahy F, Hoggard P, Back D, Barry M (2004) Intracellular accumulation of nelfinavir and its relationship to P-glycoprotein expression and function in HIV-infected patients. *Antivir Ther* **9**: 115-22
26. Ford J, Cornforth D, Hoggard PG, Cuthbertson Z, Meaden ER, Williams I, Johnson M, Daniels E, Hsyu P, Back DJ*, et al.* (2004) Intracellular and plasma pharmacokinetics of nelfinavir and M8 in HIV-infected patients: relationship with P-glycoprotein expression. *Antivir Ther* **9**: 77-84
27. Browne GJ, Finn SG, Proud CG (2004) Stimulation of the AMP-activated protein kinase leads to activation of eukaryotic elongation factor 2 kinase and to its phosphorylation at a novel site, serine 398. *The Journal of biological chemistry* **279**: 12220-31
28. Gwinn DM, Shackelford DB, Egan DF, Mihaylova MM, Mery A, Vasquez DS, Turk BE, Shaw RJ (2008) AMPK phosphorylation of raptor mediates a metabolic checkpoint. *Mol Cell* **30**: 214-26
29. Inoki K, Zhu T, Guan KL (2003) TSC2 mediates cellular energy response to control cell growth and survival. *Cell* **115**: 577-90

30. Wang X, Regufe da Mota S, Liu R, Moore CE, Xie J, Lanucara F, Agarwala U, Pyr Dit Ruys S, Vertommen D, Rider MH*, et al.* (2014) Eukaryotic elongation factor 2 kinase activity is controlled by multiple inputs from oncogenic signaling. *Mol Cell Biol* **34**: 4088-103
31. Yang Y, Ikezoe T, Takeuchi T, Adachi Y, Ohtsuki Y, Takeuchi S, Koeffler HP, Taguchi H (2005) HIV-1 protease inhibitor induces growth arrest and apoptosis of human prostate cancer LNCaP cells in vitro and in vivo in conjunction with blockade of androgen receptor STAT3 and AKT signaling. *Cancer Sci* **96**: 425-33
32. Gupta AK, Cerniglia GJ, Mick R, McKenna WG, Muschel RJ (2005) HIV protease inhibitors block Akt signaling and radiosensitize tumor cells both in vitro and in vivo. *Cancer research* **65**: 8256-65
33. Demeshkina N, Hirokawa G, Kaji A, Kaji H (2007) Novel activity of eukaryotic translocase, eEF2: dissociation of the 80S ribosome into subunits with ATP but not with GTP. *Nucleic acids research* **35**: 4597-607
34. Fan H, Penman S (1970) Regulation of protein synthesis in mammalian cells. II. Inhibition of protein synthesis at the level of initiation during mitosis. *Journal of molecular biology* **50**: 655-70
35. Gills JJ, Lopiccolo J, Dennis PA (2008) Nelfinavir, a new anti-cancer drug with pleiotropic effects and many paths to autophagy. *Autophagy* **4**: 107-9
36. Grob P, Schijns VE, van den Broek MF, Cox SP, Ackermann M, Suter M (1999) Role of the individual interferon systems and specific immunity in mice in controlling systemic dissemination of attenuated pseudorabies virus infection. *J Virol* **73**: 4748-54
37. Leprivier G, Remke M, Rotblat B, Dubuc A, Mateo AR, Kool M, Agnihotri S, El-Naggar A, Yu B, Somasekharan SP*, et al.* (2013) The eEF2 kinase confers resistance to nutrient deprivation by blocking translation elongation. *Cell* **153**: 1064-79
38. Fu LL, Xie T, Zhang SY, Liu B (2014) Eukaryotic elongation factor-2 kinase (eEF2K): a potential therapeutic target in cancer. *Apoptosis* **19**: 1527-31
39. Liu JC, Voisin V, Wang S, Wang DY, Jones RA, Datti A, Uehling D, Al-awar R, Egan SE, Bader GD*, et al.* (2014) Combined deletion of Pten and p53 in mammary epithelium accelerates triple-negative breast cancer with dependency on eEF2K. *EMBO Mol Med* **6**: 1542-60
40. Leprivier G, Rotblat B, Khan D, Jan E, Sorensen PH (2014) Stress-mediated translational control in cancer cells. *Biochim Biophys Acta*
41. Maurel M, McGrath EP, Mnich K, Healy S, Chevet E, Samali A (2015) Controlling the unfolded protein response-mediated life and death decisions in cancer. *Semin Cancer Biol* **33**: 57-66
42. Pelletier J, Graff J, Ruggero D, Sonenberg N (2015) Targeting the eIF4F translation initiation complex: a critical nexus for cancer development. *Cancer research* **75**: 250-63
43. Efeyan A, Sabatini DM (2010) mTOR and cancer: many loops in one pathway. *Curr Opin Cell Biol* **22**: 169-76
44. Liu R, Proud CG (2016) Eukaryotic elongation factor 2 kinase as a drug target in cancer, and in cardiovascular and neurodegenerative diseases. *Acta pharmacologica Sinica* **37**: 285-94
45. Randolph JT, DeGoey DA (2004) Peptidomimetic inhibitors of HIV protease. *Curr Top Med Chem* **4**: 1079-95
46. Ruggero D (2013) Translational control in cancer etiology. *Cold Spring Harbor perspectives in biology* **5**
47. Truitt ML, Conn CS, Shi Z, Pang X, Tokuyasu T, Coady AM, Seo Y, Barna M, Ruggero D (2015) Differential Requirements for eIF4E Dose in Normal Development and Cancer. *Cell* **162**: 59-71
48. Bhat M, Robichaud N, Hulea L, Sonenberg N, Pelletier J, Topisirovic I (2015) Targeting the translation machinery in cancer. *Nat Rev Drug Discov* **14**: 261-78

Figure Legends

Figure 1. Resistance to Nelfinavir triggers eEF2K down-regulation.

- **A** Molecular structure of the HIV-PI Nelfinavir (NFR) and schematic representation of the protocol used to generate NFR resistant clones. HeLa cells were maintained with 10 μM NFR. After 15 days, few clones proliferating in the constant presence of 10μM NFR in the culture medium were selected and expended for further analysis.

- **B** Dose response curves for viability of parental cells (in red) or selected clones (in black) upon treatment with NFR for 48h. The green dashed box highlight concentration in the physiologically relevant range. Curves are mean ± s.e.m. of 3 independent experiments performed in triplicate. P values were calculated using 2way ANOVA analysis of variance between parental cells and each individual clone. Bar graph represents the EC50 (half maximal effective concentration) of the dose responses. Data are mean ± s.e.m. of 3 independent experiments performed in triplicate. P values were calculated using 1way ANOVA analysis of variance (P value in red) followed by Dunnett's multiple comparison tests. **P* value ≤ 0.05, ** *P* value ≤ 0.01.

- **C** The parental population and the NFR resistant clones were analyzed for *eEF2K* mRNA expression by real-time PCR relative to β-actin (mean and s.e.m. from 3 independent batches of cells are shown). P values were calculated using 1way ANOVA analysis of variance followed by Dunnett's multiple comparison tests. **P* value ≤ 0.05, ** *P* value ≤ 0.01, *** *P* value ≤ 0.001.

- **D** The parental population and representative NFR resistant clones were analyzed by WB for eFF2K total protein level. Tubulin is used as loading control. Histogram represents mean and s.e.m of relative eEF2K level quantified from WB of 4 different batches of cells collected at different dates (see also source data). P values were calculated using 1way ANOVA analysis of variance followed by Dunnett's multiple comparison tests. *** *P* value ≤ 0.001.

Figure 2. **HIV-PIs induces eEF2K dependent eEF2 phosphorylation**.

- **A** Immunoblot analysis of eEF2 Thr^{56} phosphorylation (P-eEF2) in HeLa cells treated for 6h with increasing doses of NFR, and compared with 10 μg/ml tunicamycin (TM), 200 nM rapamycin (Rapa.) or 1h starvation (Starv.). Tubulin is used as loading control.

- **B** eEF2K WT and KO MEF treated for 6h with indicated concentration of NFR, 200 nM rapamycin (Rapa.), 1h starvation (Starv.) or 1 mM of the AMPK activator AICAR, were analyzed by immunoblot with antibodies directed against total or phosphorylated eEF2 (Thr^{56}).

- **C** Three representative NFR-resistant HeLa clones were analyzed by Immunoblot for eEF2K expression level and eEF2 phosphorylation upon NFR and compared to parental HeLa cells. For treatments, medium was replaced for 6h with medium containing DMSO (Mock), increasing doses of NFR or 10 μg/ml tunicamycin (TM), or for 1h with PBS for starvation (Starv.). Tubulin is used as loading control.

- **D** Immunoblot analysis of eEF2 Thr^{56} phosphorylation in HeLa cells treated for 6h with increasing doses of different HIV-PIs as indicated or the NFR metabolite M8 (hydroxy-tert-butylamide). Molecular structures of the different HIV-PIs used are indicated. Each panel is representative of at least 3 independent experiments.

Figure 3. NFR-mediated eEF2 phosphorylation is AMPK and mTOR independent.

- **A** Schematic representation of signaling pathways targeted by the inhibitors used in this study.

- **B** eEF2K WT and KO MEF treated for 6h with indicated concentration of NFR, Rapamycin (Rapa), AICAR or starved for indicated time in PBS (Starv.), were analyzed by immunoblot using indicated antibodies. Tubulin is used as loading control.

- **C** A potent mTOR inhibition does not impair NFR-mediated eEF2 phosphorylation. WT MEFs were treated with the indicated concentrations of Rapamycin or with vehicle (Mock). After 30 minutes, indicated doses of NFR were added and cells were incubated for additional 6h and analyzed for phosphorylated S6R and eEF2. Tubulin is used as loading control.

- **D** NFR-mediated eEF2 phosphorylation is not affected in AMPKα1α2 dKO. AMPKα1α2 WT and dKO MEF treated for 6h with indicated concentration of NFR, Rapamycin (Rapa), AICAR or starved for 1h in PBS (Starv.), were analyzed by immuoblot with indicated antibodies. * anti-total AMPKα antibody give an unspecific band with a slightly higher molecular weight in dKO cells. Tubulin is used as loading control. Each panel is representative of at least 3 independent experiments

Figure 4. **NFR regulates translation rates by phosphorylating eEF2**.

- **A-B** EEF2K contributes to the decreased translation observed with NFR without impacting translation in presence of TM. **A.** Quantification of newly synthesized proteins at 0, 2, 4 and 6h after 20 μM NFR (left panels) or 10 μg/ml TM (right panels) treatment in MEF eEF2K +/+ and eEF2K-/-. Treated cells were labeled for 15 minutes with 35S-methionine and visualized by SDS PAGE and subsequent autoradiography. Autoradiographies from four different experiments (see also source data) were quantified and results show percentage of translation compared to untreated cells. The mean and s.e.m of four independent metabolic labeling experiments are shown. *P value ≤ 0.05, ** P value ≤ 0.01, *** P value ≤ 0.001 obtained using 2way ANOVA analysis of variance (in red) followed by Bonferroni posttest (in black). **B.** eEF2K+/+, eEF2K-/-, eIF2αWT and eIF2αS51A MEFs were treated for 6h with indicated doses of NFR, 200 nM rapamycin, or 10 μg/ml TM, or for 30 min with 10 μg/ml CHX. 35S-methionine

incorporation was measured by liquid scintillation counting. Data are shown as the percentage of translation compared to untreated cells. *P value ≤ 0.05, ** P value ≤ 0.01, *** P value ≤ 0.001 obtained using 2way ANOVA analysis of variance followed by Bonferroni posttest.

- **C** Representative polysome profiles of eEF2K WT and KO MEF treated 6h with NFR or TM. Area under curve for Sub-polysomes (S) and Polysomes (P) used to calculate the P/S ratio were indicated *(see also raw data provided)*. Bar graph represents ratio normalized to untreated cells. OD254 nm is optical density at 254 nm. Data showed mean ±s.e.m. of P/S ratio calculated from 3 independent experiments. P values were calculated using 1way ANOVA analysis of variance followed by Bonferroni posttest; *P value ≤ 0.05, ** P value ≤ 0.01.

- **D** The ribosome half-transit time in MEFs eEF2K+/+ and eEF2K-/- was determined as described in Materials and Methods. Incorporation of 35S-Methionine into total protein within the PMS and PRS was obtained by linear regression analysis. Presented graphs are representative of two (CHX 1 μg/ml for 30 min and Starvation 30 min in PBS in eEF2K+/+ cells) to four (NFR 20μM for 6h in eEF2K+/+ and eEF2K-/- cells) independent experiments. Indicated values represent the x displacement measurement (in time) between the PMS line at 300sec and the PRS line *(see also raw data provided)*. Histogram represents mean and s.e.m. of the ribosome half transit time from four independent experiments. P values were calculated using two tails unpaired Student's T-tests; *P value ≤ 0.05.

Figure 5. **NFR mediated eEF2K activation impairs cell proliferation and triggers cell death**.

- **A** MEF eEF2K WT, KO or KO reconstituted with human eFF2K (FlageEF2K) were analyzed for cell growth at indicated times. Fold change (means ± s.e.m of triplicate) of the cell number just before treatment are shown. Histogram shows percentage of growth inhibition after 72h of 10 μM NFR. P values are 1way ANOVA with Bonferroni posttest calculated from 3 independent experiments. *** P value ≤ 0.001.

- **B-F** Dose response curves for cell viability after 48h NFR measured using MTS assay. Curves and bar graph for EC50 are mean ± s.e.m. of 3 independent experiments performed in triplicate. For curves, p values are 2way ANOVA analysis of variance. For bar graph, p values are two tails unpaired Student's T-tests (B, E), or 1way ANOVA with Bonferroni (C) or Dunnett's multiple comparison posttests (D and F). *P value ≤ 0.05, ** P value ≤ 0.01, *** P value ≤ 0.001. (**B,C**) eEF2K -/- MEFs show a decrease susceptibly to NFR compared to eEF2K +/+ controls (B) whereas eEF2K reconstitution restores NFR sensitivity (C). (**D-F**), HeLa (D), A549 (E) and MCF7 (F) clones with CRISPR-Cas9 generated eEF2K deficiency (CrEEF2K) show a decrease susceptibly to NFR compare to control cells (CrLuci).

- **G** NFR-mediated toxicity assessed using AnnexinV/PI staining and FACS analysis after 24h treatment. Histogram shows the percentage of dead cells (AV+/PI+). Data are mean

± s.e.m. of 3 independent experiments. P values are 2way ANOVA with Bonferroni posttest. *P value ≤ 0.05, ** P value ≤ 0.01, *** P value ≤ 0.001.

Figure 6. **eEF2K is required for NFR-mediated antitumoral activity.**

- **A** Tumor volumes of eEF2K -/- and eEF2K +/+ Ras^{V12} engraft implanted subcutaneously in AGR129 mice. Treatment with NFR or vehicle was initiated 6 days post-implantation. Data are mean of tumor volume ± s.e.m. (n = 8 per group). P values were calculated using 2way ANOVA followed by Bonferroni posttest comparing WT tumor with vehicle or NFR treatment and KO tumors with vehicle or NFR treatment; *P value ≤ 0.05, ** P value ≤ 0.01, *** P value ≤ 0.001. Experiment is representative of 2 performed in same conditions.

- **B** Immunoblots for total and phosphorylated eEF2 of tumor engraftment from (A). **(**NS, Non-Specific signal.)

- **C** Bar graph shows relative phosphorylation intensities of eEF2 compared with total eEF2 determined by densitometry analysis. Mean ± s.e.m. are shown (n=4). P values were calculated using 2way ANOVA followed by Bonferroni posttest ; **P value ≤ 0.01.

Expanded View Figure Legends

Figure EV1. eEF2K decreased level in NFR-resistant HeLa clones.

- NFR was washout from resistant clones culture medium for indicated times and cells were harvested and analyzed for eEF2K protein level. Below numbers represent the relative eEF2K expression compare to untreated parental cell line and were obtained by WB quantification normalizing eEF2K on tubulin levels.

Figure EV2. eEF2K deficiency does not impair NFR mediated ISR induction and *vice versa*.

- **A** Activation of the integrated stress response by NFR was not affected by eEF2K deficiency. ISR activation was measured in eEF2K -/- MEFs and eEF2K +/+ MEFs by immunobloting of the translation factor ATF4 and the phosphorylation of the initiation factor eIF2α. NFR response (6h treatment) was compared with treatments using 10 μg/ml tunicamycin (TM), an inducer of the integrated stress response, 200 nM rapamycin (Rapa.) or 1h of starvation in PBS (Starv.). Tubulin is used as loading control.
- **B** NFR mediates eEF2 phosphorylation independently from eIF2α phosphorylation, the effector of the ISR. NFR response was analyzed in eIF2α WT MEFs and cells unable to

carry eIF2α phosphorylation on Ser^{51} (eIF2αS51A). Immunoblot analysis was performed to assess the phosphorylation of eEF2 and eIF2α as well as ATF4 expression after 6h treatment with indicated dose of NFR, 10 μg/ml tunicamycin (TM) and 200 nM rapamycin (Rapa.) and after 1h of starvation (Starv.). Tubulin is used as loading control. Each panel is representative of at least 3 independent experiments.

Figure EV3. ISR is not affected in NFR resistant clones and NFR triggers eEF2 phosphorylation independently of Akt.

- **A** Three representative NFR-resistant HeLa clones were analyzed by Immunoblot for eEF2 phosphorylation upon NFR and compared to parental HeLa cells (see Fig 2). Histogram shows the mean and s.e.m. of p-eEF2/tot-eEF2 ratio obtained from WB quantification of three independent experiments. Data were normalized using NFR 40μM treated parental cell line as the maximum (100%) p-eEF2 signal for each individual experiment.

- **B** Immunoblot analysis of NFR mediated activation of ER-stress markers in three NFR-resistant HeLa clones compared to parental HeLa cells. EIF2α phosphorylation, and expression of ATF4 are shown. For treatments, medium was replaced for 6h with medium containing increasing doses of NFR or 10 mg/ml tunicamycin (TM), or for 1h with PBS for starvation (Starv.) This experiment is representative of 3.

- **C** NFR resistant clones and parental HeLa cells were analyzed for expression of the stress factors CHOP and DNAjB9 by real-time PCR relative to β-actin (mean and s.e.m. from 3 independent batches of cells are shown). P values were calculated using 1way ANOVA analysis of variance followed by Dunnett's multiple comparison test; *P value ≤ 0.05, ** P value ≤ 0.01, *** P value ≤ 0.001.

- **D** eEF2K phosphorylation was measured using phos-tag SDS-PAGE and specific antibodies in HeLa cells subjected to indicated treatments. This experiment is representative of 3.

- **E** MK2206-mediated Akt inhibition does not affect NFR ability to induce eEF2 phosphorylation. MEFs were treated with indicated concentration of the potent Akt inhibitor MK2206 or left untreated. After 30 minutes NFR was added for additional 6h. Immunoblot analysis was performed for phosphorylated and total Akt and eEF2 as indicated. Panel is representative of 3 independent experiments. Tubulin is used as loading control.

Figure EV4. NFR mediated changes in polysomal profile is not dependent on eIF2α phosphorylation.

- **A** Representative polysome profiles of WT MEFs treated 6h with NFR or TM with or without 500 nM ISRIB. Bar graph represents the ratio of sub-polysomes compared with polysomes (P/S). OD254 nm is optical density at 254 nm. Data showed mean ±s.e.m. of P/S ratio calculated from 2 independent experiments. P values were calculated using two

tails unpaired Student's T-tests comparing ratio +/- ISRIB; *P value ≤ 0.05. ISRIB efficiency at inhibiting NFR or TM mediated ATF4 induction was tested by immunoblot.

- **B-C** Representative polysome profiles of eIF2αWT and eIF2αS51A MEFs treated 6h with NFR or TM (B) or WT MEFs treated for 6h with 20 μM NFR or 200 nM Rapamycin (C, upper panel) or 30 min with 1 μg/ml CHX (C, lower panel). Data showed mean ±s.e.m. of P/S ratio calculated from 2 to 3 independent experiments. P values were calculated using 1way ANOVA analysis of variance followed by Bonferroni posttest (B and C, upper panel) or two tails unpaired Student's T-tests (C, lower panel); *P value ≤ 0.05, ** P value ≤ 0.01.

Figure EV5. UPR deficiency does not improve viability in presence of NFR.

Dose response curves for cell viability in MEFs unable to phosphorylate eIF2α (eIF2αS51A) or deficient for PERK, ATF4, IRE1, XBP1, and respective control cells treated with increasing doses of NFR for 48h. Dose response curves for cell viability. Bar graph represents the EC50 (half maximal effective concentration) of the dose responses. Data are mean ± s.e.m. of 3 independent experiments performed in triplicate. Statistical significance was assessed using 2way ANOVA analysis of variance for dose response and two tails unpaired Student's T-tests for EC50. No significant differences were measured in the tested cell lines.

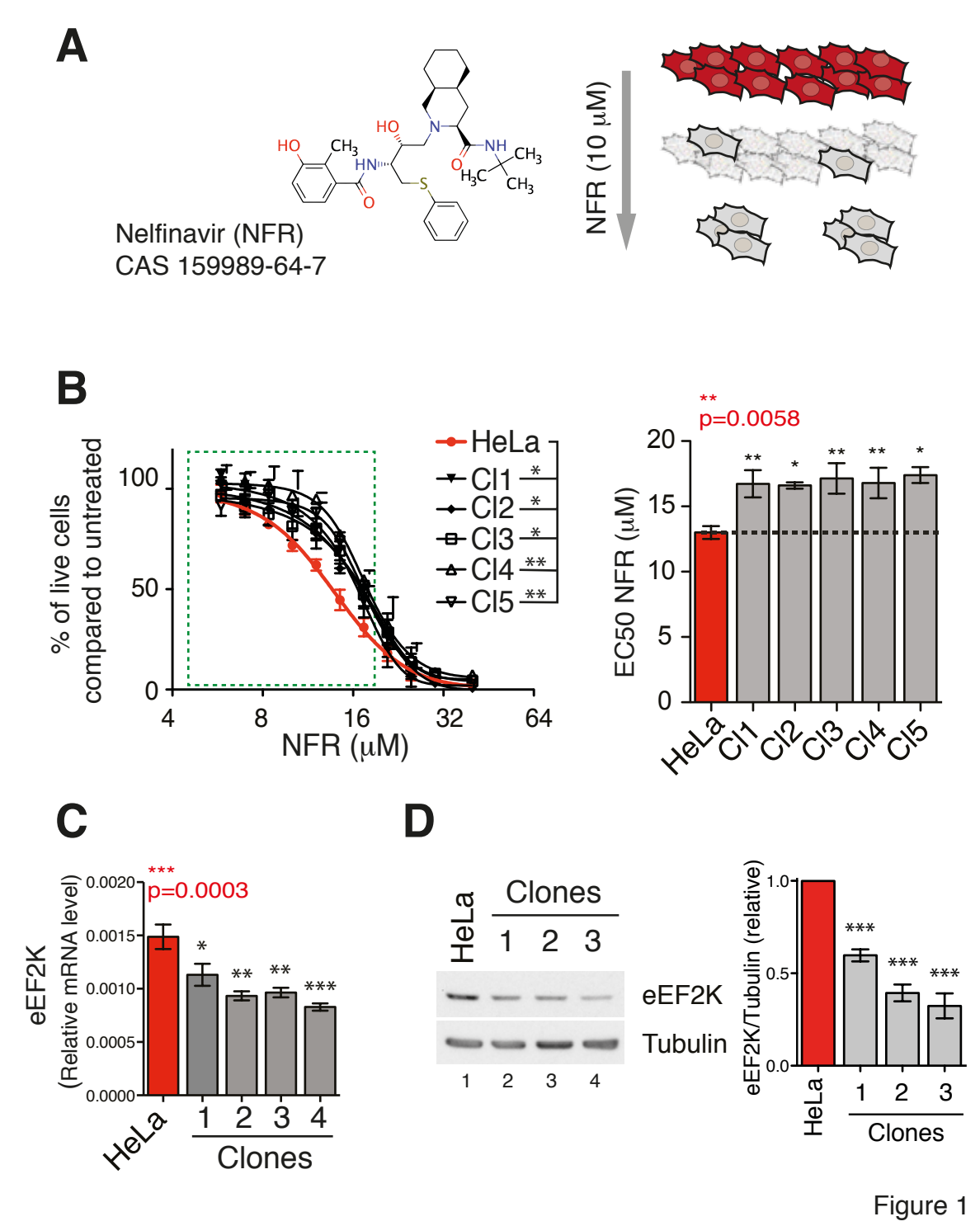
A
Nelfinavir (NFR)
CAS 159989-64-7
NFR (10 μM)
B
% of live cells compared to untreated
NFR (μM)
HeLa
Cl1
Cl2
Cl3
Cl4
Cl5
p=0.0058
EC50 NFR (μM)
C
eEF2K (Relative mRNA level)
p=0.0003
Clones
D
Clones
eEF2K
Tubulin
eEF2K/Tubulin (relative)

Figure 1

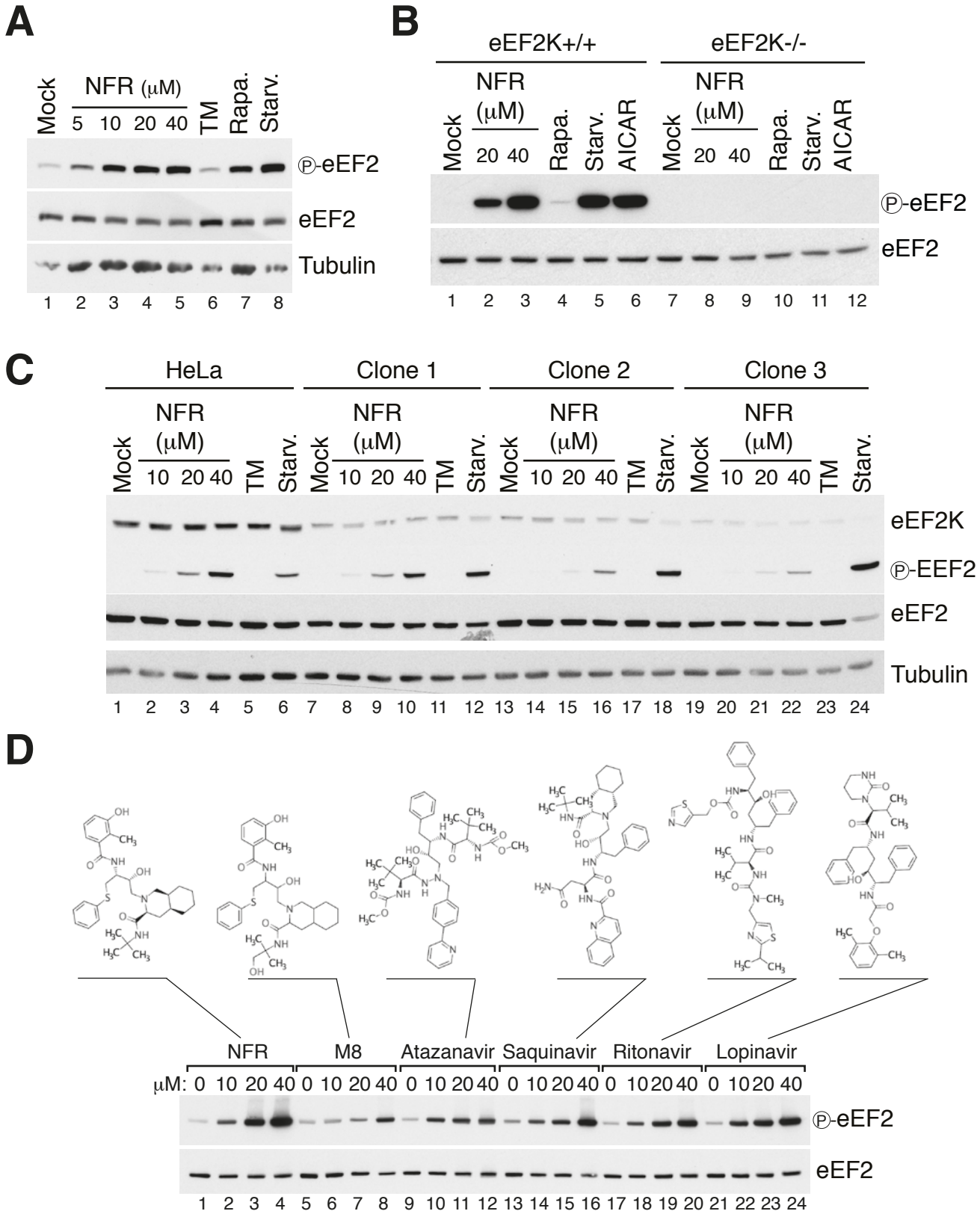
A
Mock
NFR (μM)
5 10 20 40
TM
Rapa.
Starv.
Ⓟ-eEF2
eEF2
Tubulin
1 2 3 4 5 6 7 8
B
eEF2K+/+
eEF2K-/-
Mock
NFR (μM)
20 40
Rapa.
Starv.
AICAR
Ⓟ-eEF2
eEF2
1 2 3 4 5 6 7 8 9 10 11 12
C
HeLa
Clone 1
Clone 2
Clone 3
Mock
NFR (μM)
10 20 40
TM
Starv.
eEF2K
Ⓟ-EEF2
eEF2
Tubulin
1 2 3 4 5 6 7 8 9 10 11 12 13 14 15 16 17 18 19 20 21 22 23 24
D
NFR
M8
Atazanavir
Saquinavir
Ritonavir
Lopinavir
μM: 0 10 20 40 0 10 20 40 0 10 20 40 0 10 20 40 0 10 20 40 0 10 20 40
Ⓟ-eEF2
eEF2
1 2 3 4 5 6 7 8 9 10 11 12 13 14 15 16 17 18 19 20 21 22 23 24

Figure 2

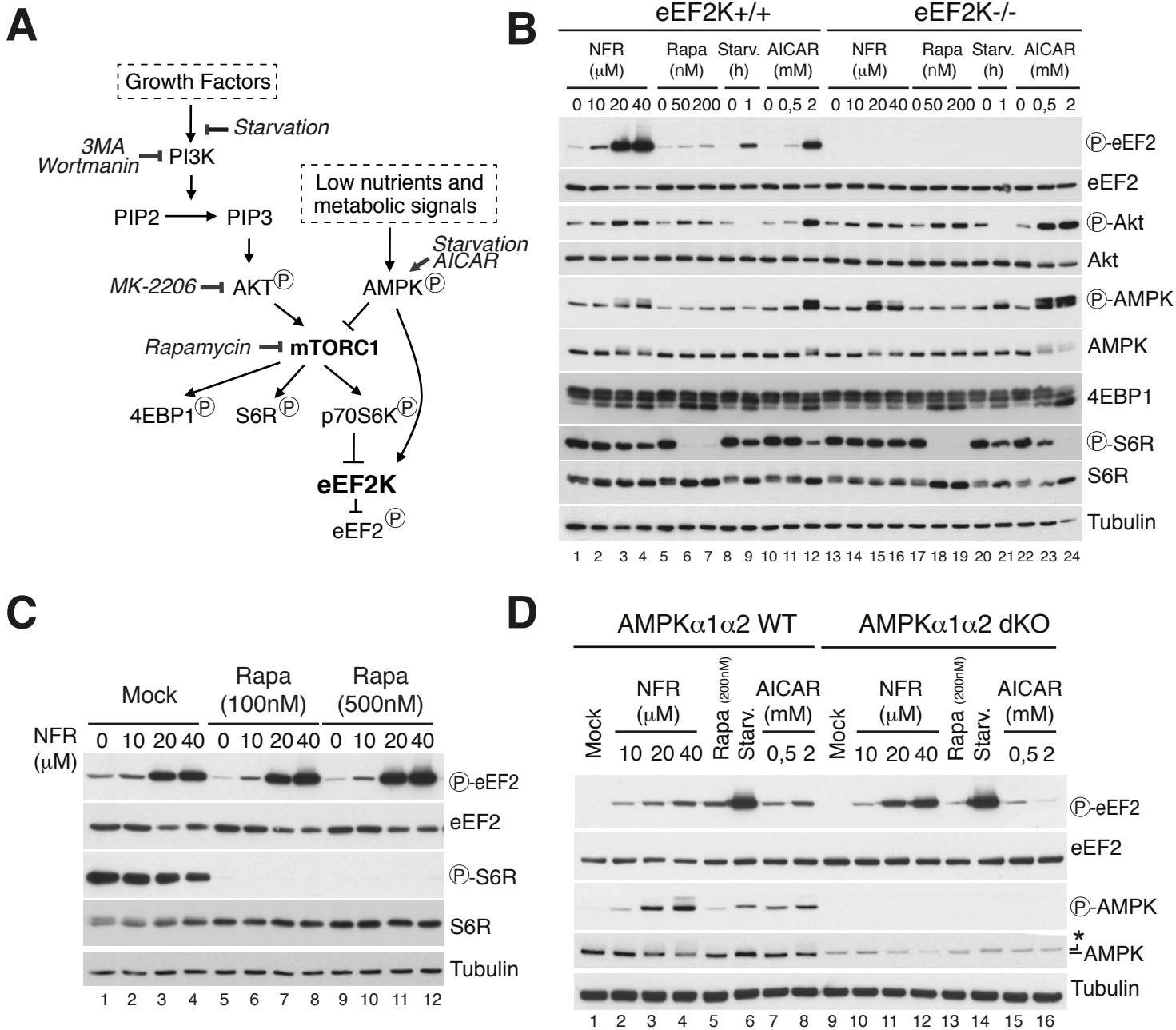
A
Growth Factors
Starvation
3MA
Wortmanin
PI3K
PIP2
PIP3
Low nutrients and
metabolic signals
Starvation
AICAR
MK-2206
AKT Ⓟ
AMPK Ⓟ
Rapamycin
mTORC1
4EBP1 Ⓟ
S6R Ⓟ
p70S6K Ⓟ
eEF2K
eEF2 Ⓟ
B
eEF2K+/+
eEF2K-/-
NFR (μM)
Rapa (nM)
Starv. (h)
AICAR (mM)
0 10 20 40 0 50 200 0 1 0 0,5 2
0 10 20 40 0 50 200 0 1 0 0,5 2
Ⓟ-eEF2
eEF2
Ⓟ-Akt
Akt
Ⓟ-AMPK
AMPK
4EBP1
Ⓟ-S6R
S6R
Tubulin
1 2 3 4 5 6 7 8 9 10 11 12 13 14 15 16 17 18 19 20 21 22 23 24
C
Mock
Rapa (100nM)
Rapa (500nM)
NFR (μM)
0 10 20 40 0 10 20 40 0 10 20 40
Ⓟ-eEF2
eEF2
Ⓟ-S6R
S6R
Tubulin
1 2 3 4 5 6 7 8 9 10 11 12
D
AMPKα1α2 WT
AMPKα1α2 dKO
Mock
NFR (μM)
Rapa (200nM)
Starv.
AICAR (mM)
10 20 40
0,5 2
Ⓟ-eEF2
eEF2
Ⓟ-AMPK
*AMPK
Tubulin
1 2 3 4 5 6 7 8 9 10 11 12 13 14 15 16

Figure 3

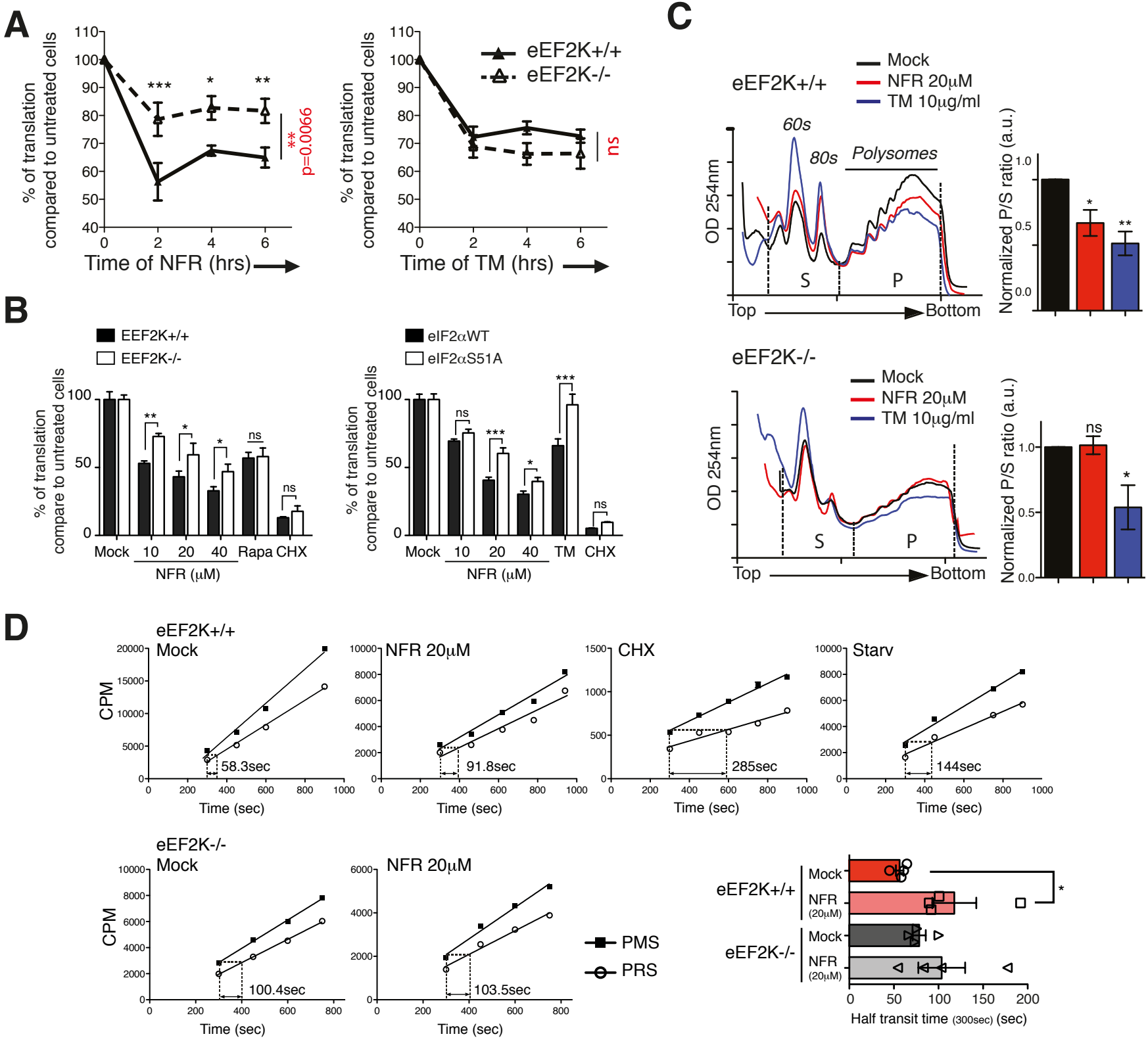
A
% of translation compared to untreated cells
Time of NFR (hrs)
Time of TM (hrs)
eEF2K+/+
eEF2K-/-
**
p=0.0066
ns
B
EEF2K+/+
EEF2K-/-
eIF2αWT
eIF2αS51A
% of translation compare to untreated cells
Mock
10
20
40
Rapa
CHX
TM
NFR (μM)
C
eEF2K+/+
eEF2K-/-
Mock
NFR 20μM
TM 10μg/ml
60s
80s
Polysomes
OD 254nm
S
P
Top
Bottom
Normalized P/S ratio (a.u.)
D
eEF2K+/+
Mock
NFR 20μM
CHX
Starv
CPM
Time (sec)
58.3sec
91.8sec
285sec
144sec
eEF2K-/-
100.4sec
103.5sec
PMS
PRS
Half transit time (300sec) (sec)

Figure 4

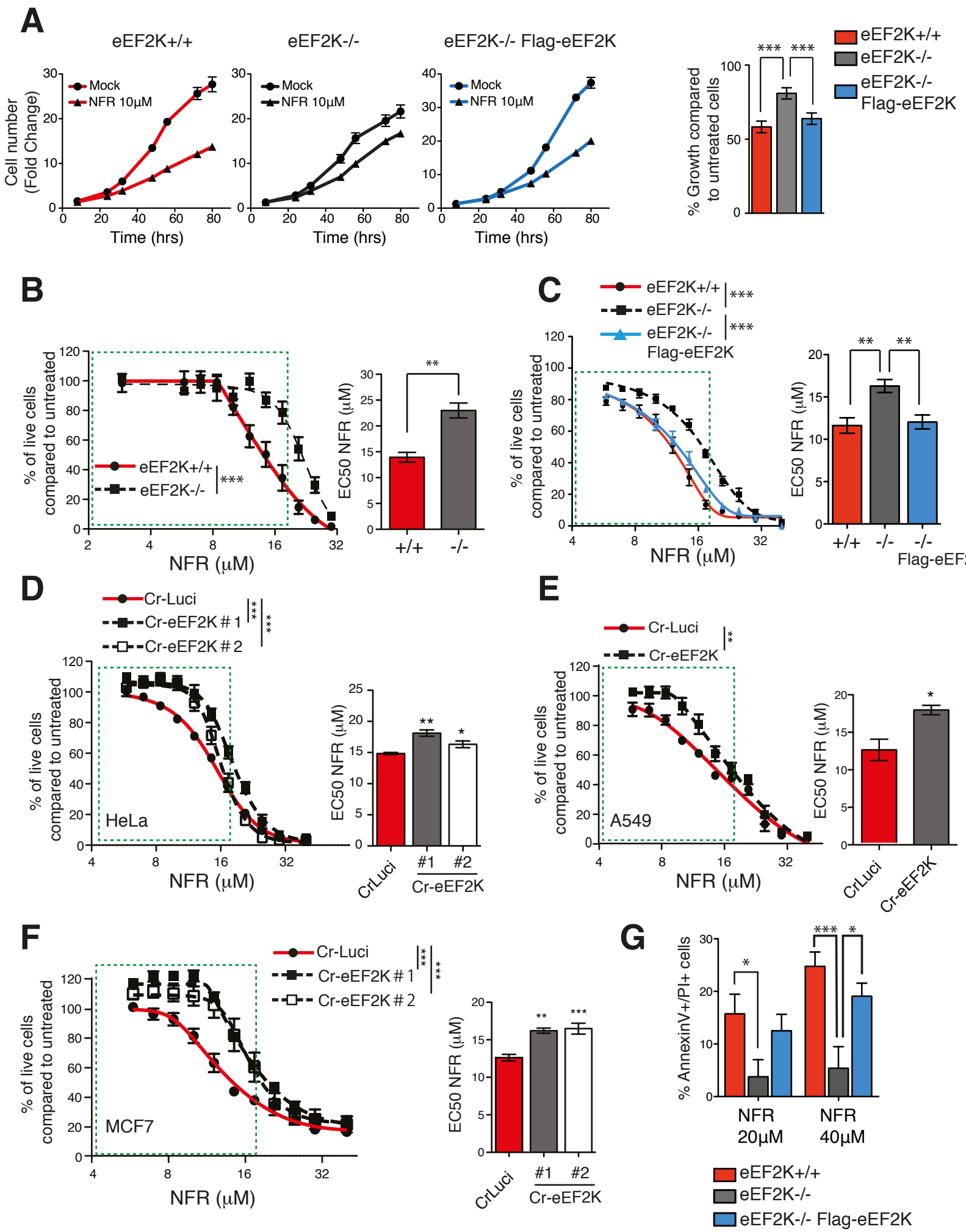
A
eEF2K+/+
eEF2K-/-
eEF2K-/- Flag-eEF2K
Mock
NFR 10μM
Cell number (Fold Change)
Time (hrs)
% Growth compared to untreated cells
***
***
eEF2K+/+
eEF2K-/-
eEF2K-/- Flag-eEF2K
B
% of live cells compared to untreated
NFR (μM)
eEF2K+/+
eEF2K-/-
***
EC50 NFR (μM)
**
+/+
-/-
C
eEF2K+/+
eEF2K-/-
eEF2K-/- Flag-eEF2K
***
***
% of live cells compared to untreated
NFR (μM)
EC50 NFR (μM)
**
**
+/+
-/-
-/- Flag-eEF2K
D
Cr-Luci
Cr-eEF2K # 1
Cr-eEF2K # 2
***
***
% of live cells compared to untreated
HeLa
NFR (μM)
EC50 NFR (μM)
**
*
CrLuci
#1
#2
Cr-eEF2K
E
Cr-Luci
Cr-eEF2K
**
% of live cells compared to untreated
A549
NFR (μM)
EC50 NFR (μM)
*
CrLuci
Cr-eEF2K
F
Cr-Luci
Cr-eEF2K # 1
Cr-eEF2K # 2
***
***
% of live cells compared to untreated
MCF7
NFR (μM)
EC50 NFR (μM)
**
***
CrLuci
#1
#2
Cr-eEF2K
G
% AnnexinV+/PI+ cells
*
***
*
NFR 20μM
NFR 40μM
eEF2K+/+
eEF2K-/-
eEF2K-/- Flag-eEF2K

Figure 5

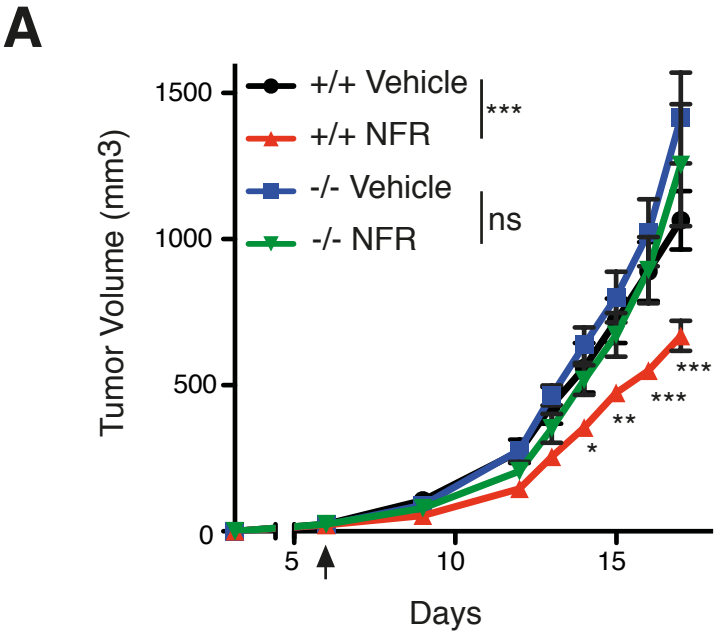
A
Tumor Volume (mm3)
1500
1000
500
0
+/+ Vehicle
+/+ NFR
-/- Vehicle
-/- NFR
***
ns
*
**
***
***
5
10
15
Days

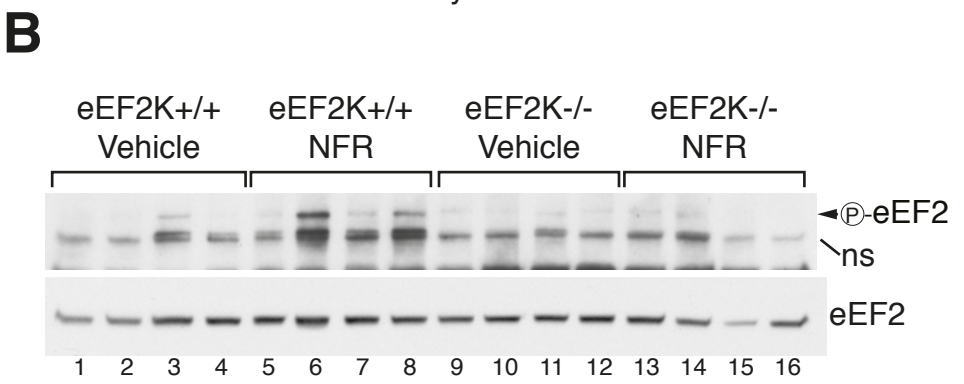
B
eEF2K+/+ Vehicle
eEF2K+/+ NFR
eEF2K-/- Vehicle
eEF2K-/- NFR
Ⓟ-eEF2
ns
eEF2
1 2 3 4 5 6 7 8 9 10 11 12 13 14 15 16

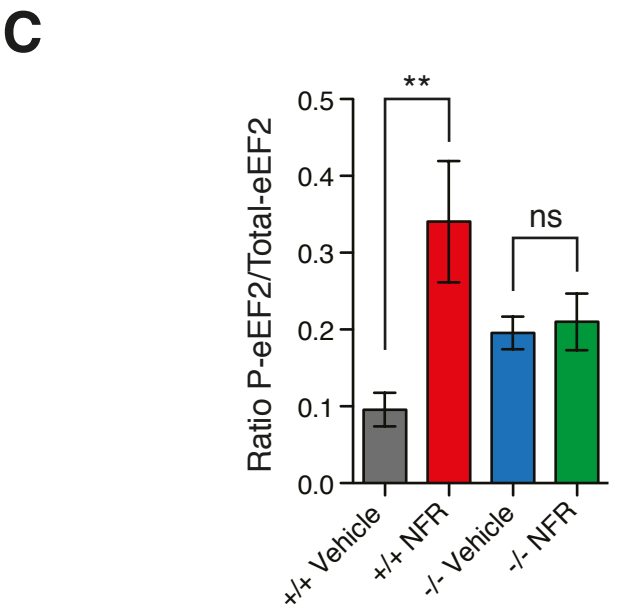
C
Ratio P-eEF2/Total-eEF2
0.5
0.4
0.3
0.2
0.1
0.0
**
ns
+/+ Vehicle
+/+ NFR
-/- Vehicle
-/- NFR

Figure 6

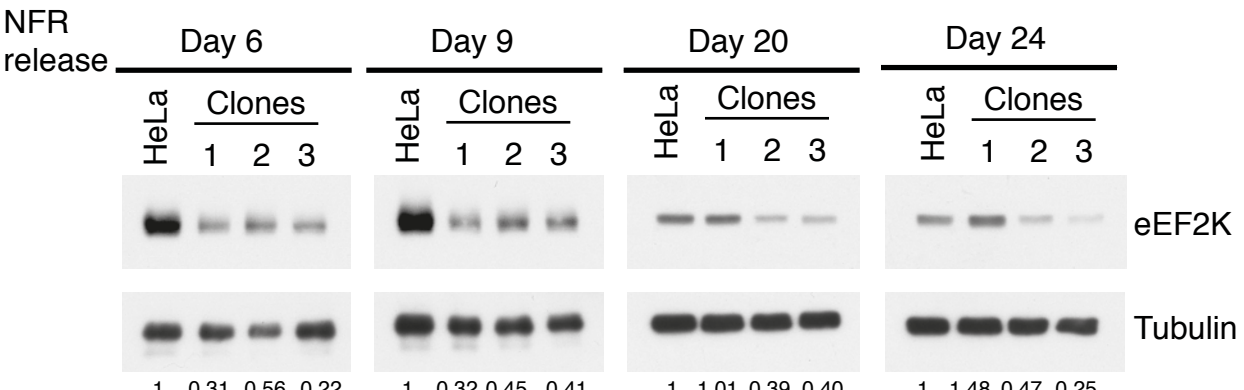
NFR release
Day 6
Day 9
Day 20
Day 24
HeLa
Clones
1 2 3
eEF2K
Tubulin
1 0.31 0.56 0.22
1 0.32 0.45 0.41
1 1,01 0.39 0.40
1 1.48 0.47 0.25

Figure EV1

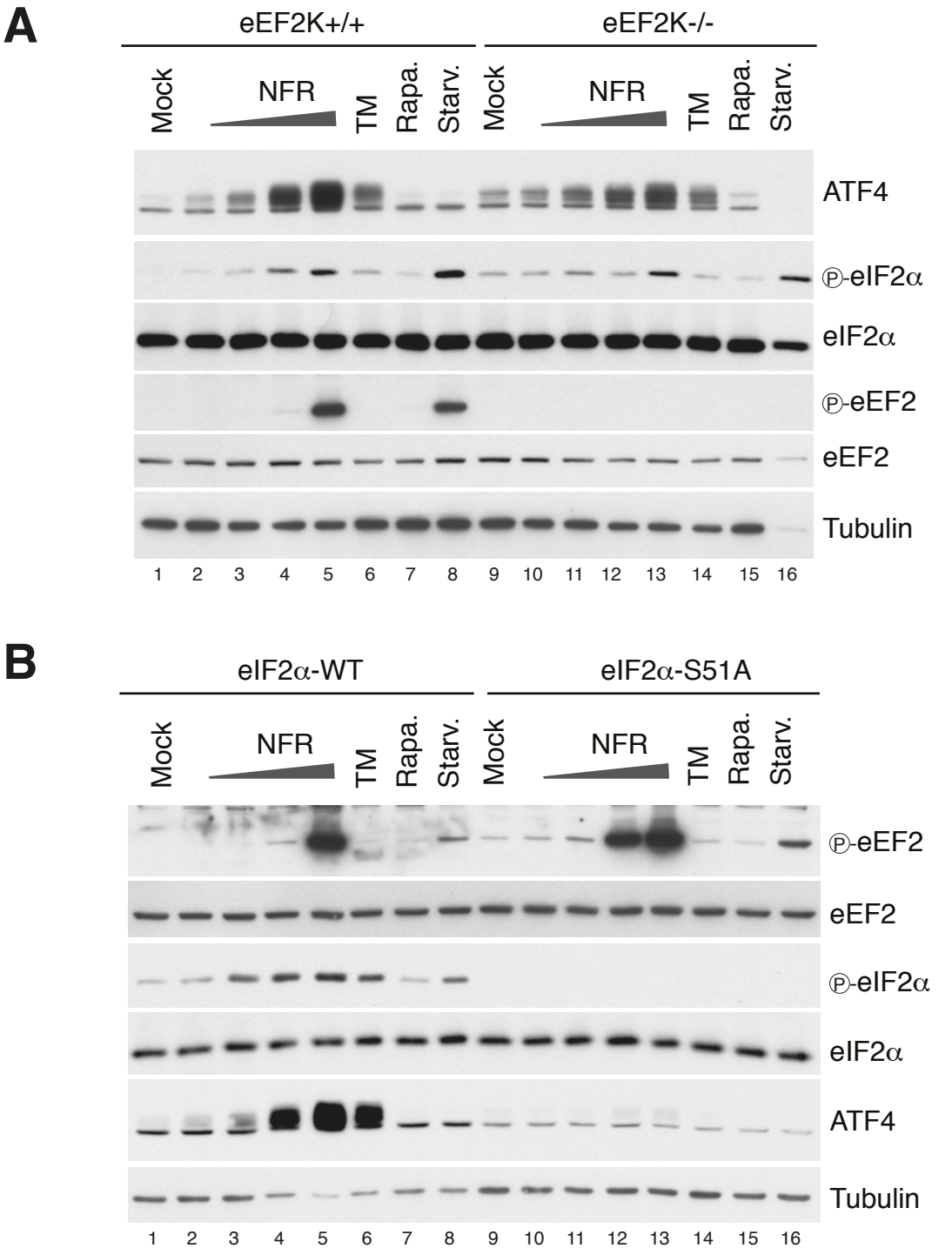
A
eEF2K+/+
eEF2K-/-
Mock
NFR
TM
Rapa.
Starv.
Mock
NFR
TM
Rapa.
Starv.
ATF4
Ⓟ-eIF2α
eIF2α
Ⓟ-eEF2
eEF2
Tubulin
1 2 3 4 5 6 7 8 9 10 11 12 13 14 15 16
B
eIF2α-WT
eIF2α-S51A
Mock
NFR
TM
Rapa.
Starv.
Mock
NFR
TM
Rapa.
Starv.
Ⓟ-eEF2
eEF2
Ⓟ-eIF2α
eIF2α
ATF4
Tubulin
1 2 3 4 5 6 7 8 9 10 11 12 13 14 15 16

Figure EV2

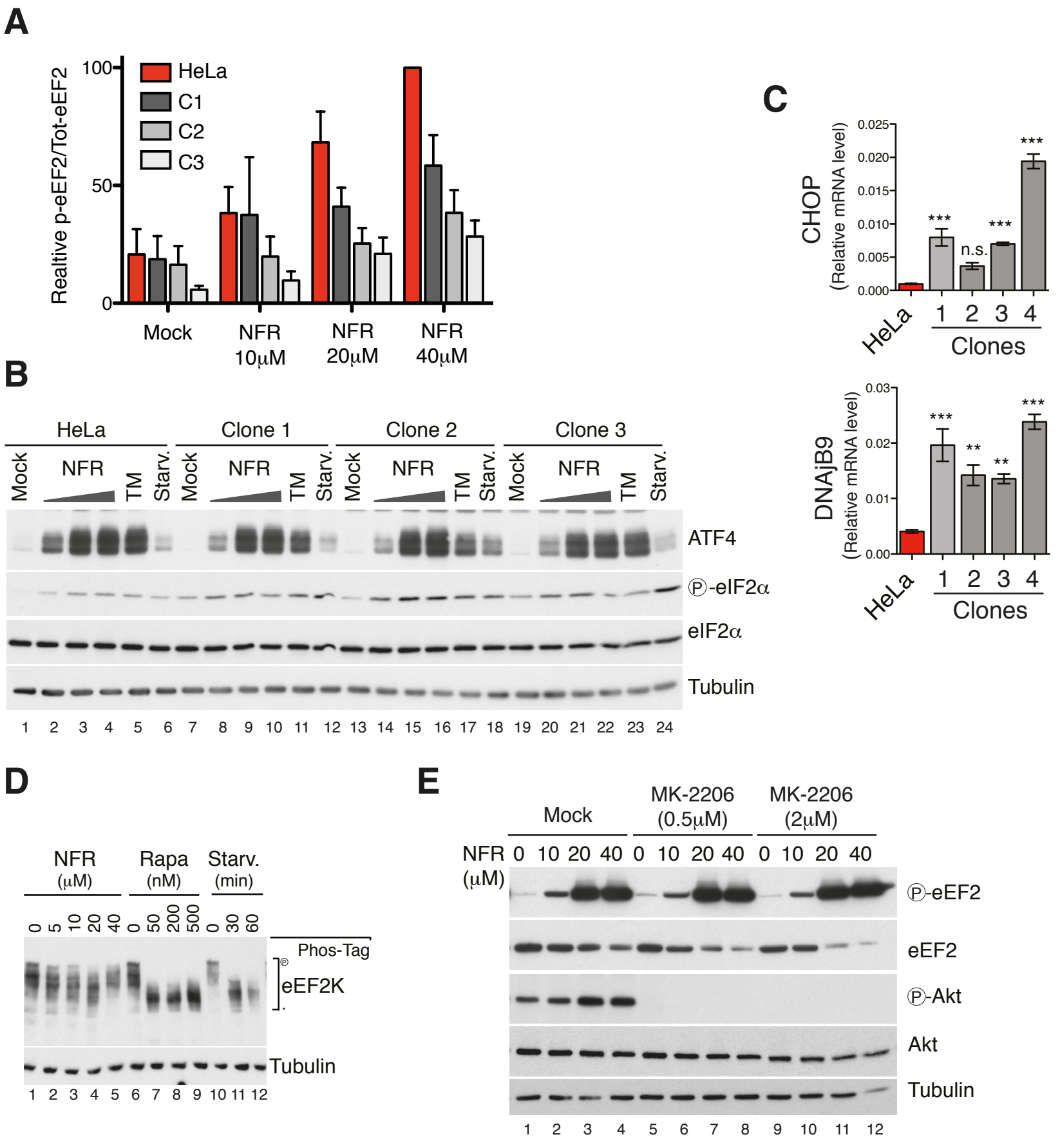
A
Realtive p-eEF2/Tot-eEF2
100
50
0
HeLa
C1
C2
C3
Mock
NFR 10μM
NFR 20μM
NFR 40μM
B
HeLa
Clone 1
Clone 2
Clone 3
Mock
NFR
TM
Starv.
ATF4
Ⓟ-eIF2α
eIF2α
Tubulin
1 2 3 4 5 6 7 8 9 10 11 12 13 14 15 16 17 18 19 20 21 22 23 24
C
CHOP
(Relative mRNA level)
0.025
0.020
0.015
0.010
0.005
0.000
***
n.s.
HeLa
1 2 3 4
Clones
DNAjB9
(Relative mRNA level)
0.03
0.02
0.01
0.00
***
**
D
NFR (μM)
Rapa (nM)
Starv. (min)
0 5 10 20 40
0 50 200 500
0 30 60
Phos-Tag
Ⓟ
eEF2K
Tubulin
1 2 3 4 5 6 7 8 9 10 11 12
E
Mock
MK-2206 (0.5μM)
MK-2206 (2μM)
NFR (μM) 0 10 20 40 0 10 20 40 0 10 20 40
Ⓟ-eEF2
eEF2
Ⓟ-Akt
Akt
Tubulin
1 2 3 4 5 6 7 8 9 10 11 12

Figure EV3

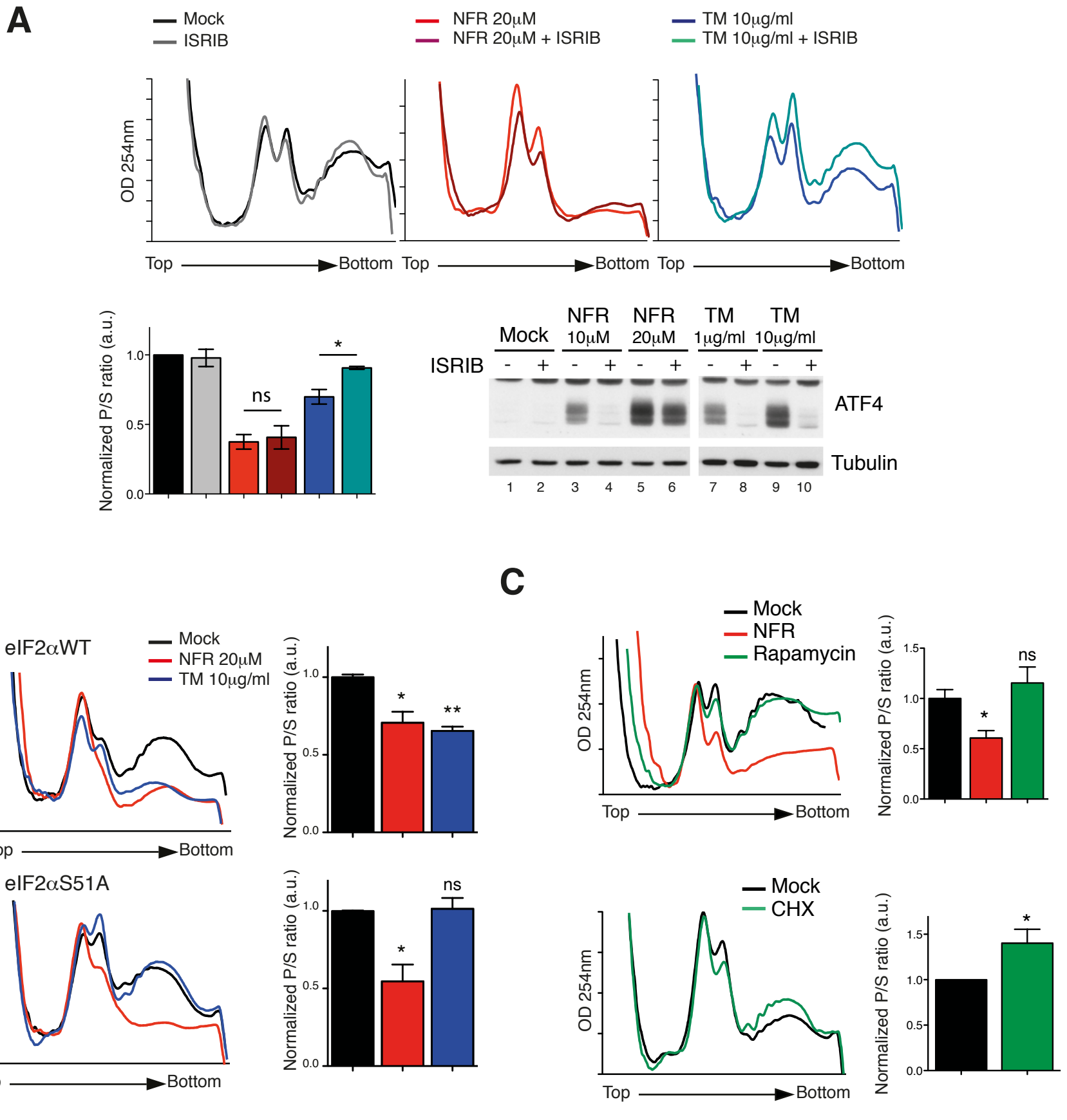
A
Mock
ISRIB
NFR 20μM
NFR 20μM + ISRIB
TM 10μg/ml
TM 10μg/ml + ISRIB
OD 254nm
Top
Bottom
Normalized P/S ratio (a.u.)
ns
*
Mock
NFR 10μM
NFR 20μM
TM 1μg/ml
TM 10μg/ml
ISRIB
ATF4
Tubulin
1 2 3 4 5 6 7 8 9 10
B
eIF2αWT
Mock
NFR 20μM
TM 10μg/ml
**
eIF2αS51A
C
Mock
NFR
Rapamycin
CHX

Figure EV4

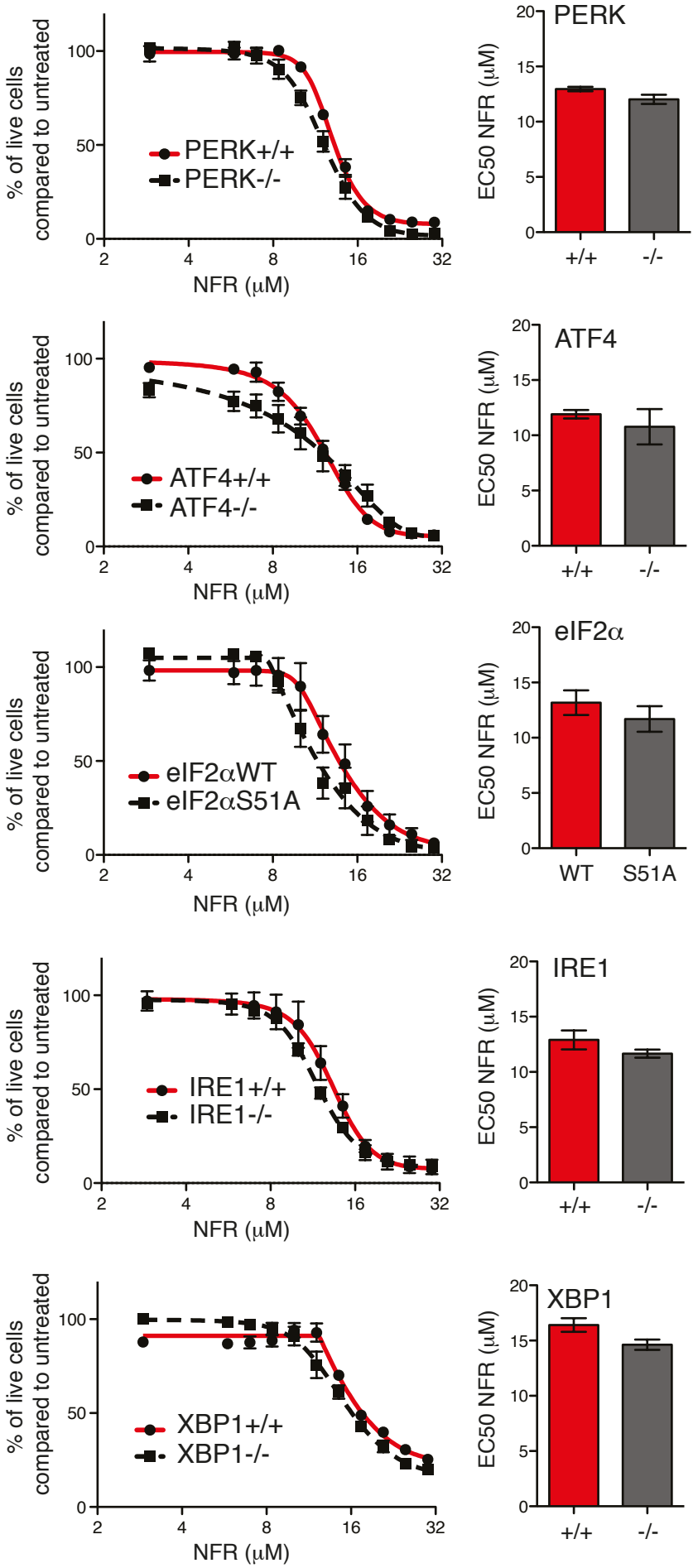
% of live cells compared to untreated
NFR (μM)
PERK+/+
PERK-/-
EC50 NFR (μM)
PERK
+/+
-/-
ATF4+/+
ATF4-/-
ATF4
eIF2αWT
eIF2αS51A
eIF2α
WT
S51A
IRE1+/+
IRE1-/-
IRE1
XBP1+/+
XBP1-/-
XBP1

Figure EV5